POLITECNICO
MILANO 1863

SCUOLA DI INGEGNERIA INDUSTRIALE
E DELL'INFORMAZIONE

Predictive maintenance of a hot forging process through vibration monitoring

TESI MAGISTRALE IN

MECHANICAL ENGINEERING – INGEGNERIA MECCANICA

Alonso Toral, Lucas, 10623951

Advisor:

Prof. Marco Tarabini

Co-advisors:

Chiara Conese

Fabio Conti

Academic year:

2021-22

Abstract:

This work applies vibration analysis to characterize the nominal working conditions of a three stages eccentric press used in a hot forging process. The characterization is successfully achieved through the analysis of time-domain features, frequency-domain features, and envelope analysis. The origin of each of the recorded vibration signals is studied, and the advantages of different frequency filters and sensor locations is discussed. Finally, a monitoring strategy for the forging process is proposed.

Key-words: forging, predictive maintenance, vibration, condition monitoring

1. Introduction

Forging is a manufacturing process in which a piece of metal is shaped by compressive forces applied with a press machine through a system of dies and tooling. In the industry we can find a wide variety of machines (hydraulic presses, crank presses, screw presses, hammers,…), techniques (open die, closed die, precision forging,…), and operating conditions (mainly cold forging and hot forging). These depend on the material used, the geometry and physical requirements of the final product, and the economic convenience of each possible setup, among other reasons [1].

The forging station studied in this thesis consists of a 1600 tons eccentric press performing a hot forging process. The kinetic energy is transferred from an electric motor to an inertia flywheel and then to the eccentric

shaft, which again transforms the rotational movement into a linear one, producing the vertical movement of the ram. The movement is only transferred from the flywheel to the ram when it is needed, being stopped most of the time in order to allow the operators to position the workpiece in the required stage. A 3D CAD model of a simplified eccentric press showing the force transmission process just described can be seen in Figure 1 [2].

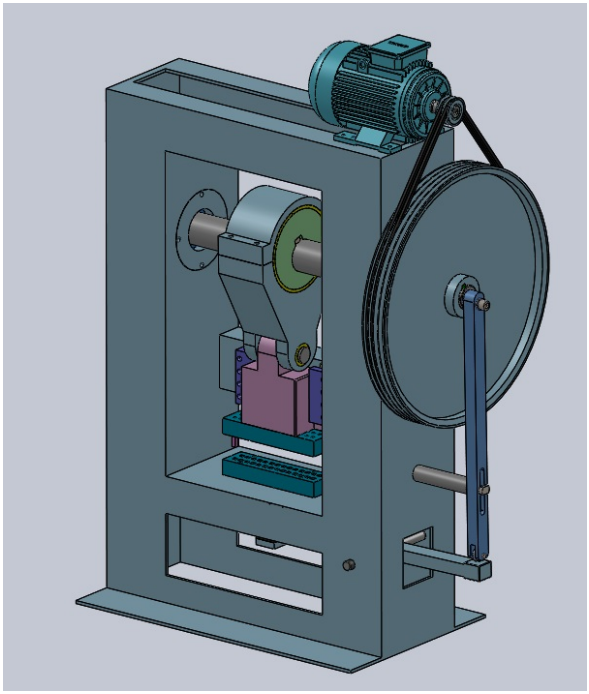

Figure 1. Simplified eccentric press [2]

The deformation from the initial steel billet to the final piece takes place through a 3-stages process: an initial preforming, the forming of the piece itself, and the removal of the flash, in a process almost identical to the points 2 to 4 shown in Figure 2 [1]. The steel billets are previously heated in an industrial furnace up to 1200°C, which allows for a significant reduction in the required forming forces with respect to an equivalent cold forging process.

The problem found by the owners of the press is that, after a substantial increase in the clearances of the machine, the eccentric shaft ends up inevitably breaking at the points marked in Figure 3 [3]. This agrees with the publications found on eccentric shaft failure in press machines: Rusiński et al. [3] indicate that eccentric presses develop fatigue cracks at the cam mounting point caused by bending and torsion stresses, forming a notch area that ultimately results in fatigue failure after 5 to 15 years of service for machines in the range of 1300 to 2500 tons (like the one being studied); while Hamrle et al. [4] point out how the placing of multiple forging stations in a single machine, driven by economic efficiency, results in a significant increase in bending stress (specially for off-centre loads). This bending stress can be partially mitigated using a two-point eccentric shaft, but the main stresses are still found in the points where the shaft diameter changes, as can be seen in Figure 4 [4].

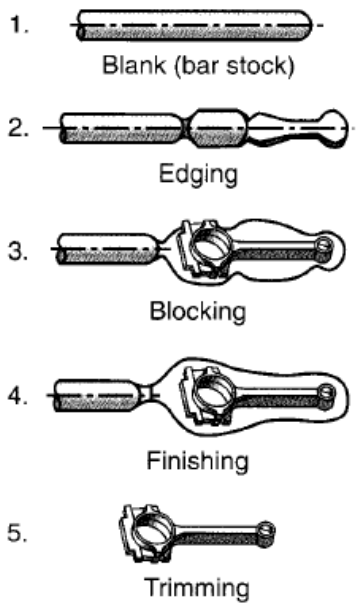

Figure 2. Stages in the forging of a connecting rod for an internal combustion engine [1].

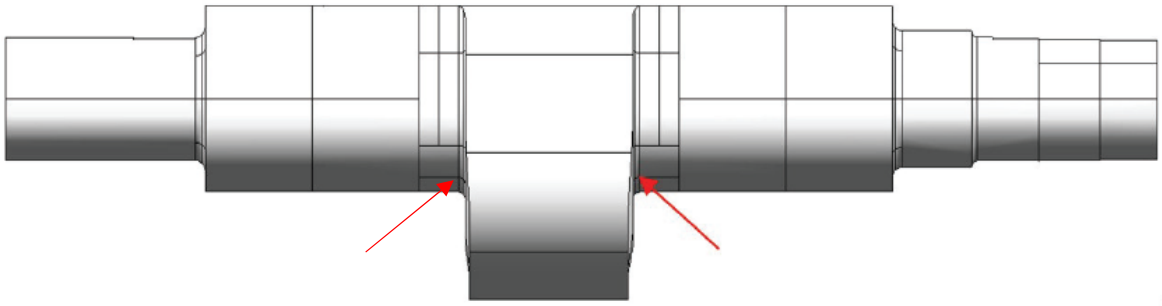

Figure 3. Areas in which the fatigue cracks start appearing, ultimately causing shaft failure [3]

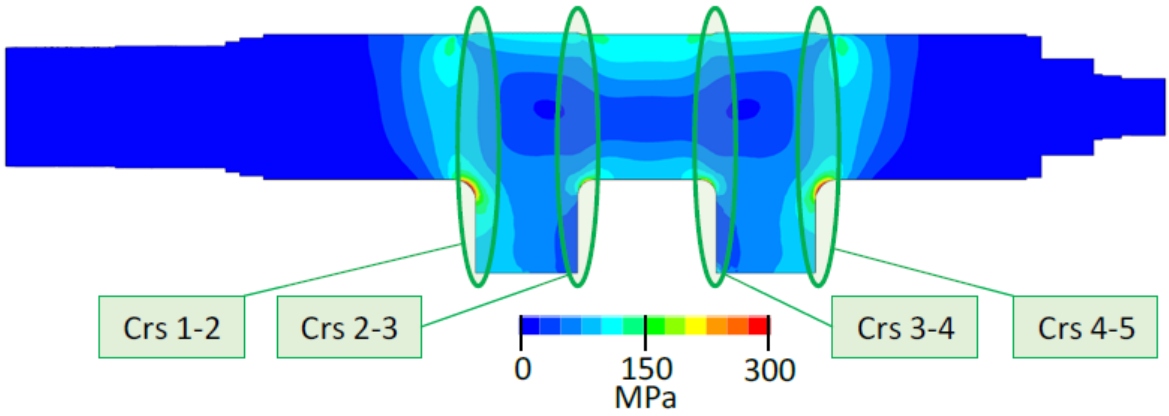

Figure 4. Von Mises stress distribution in a 2-point eccentric crankshaft [4]

As it was discussed during a meeting with the company owner of the machine and the production system, the failure of the crankshaft in an eccentric press as big as the one being studied can result, at best, in weeks or even months long periods in which the press would be completely unusable. This occurs because the process of ordering a new shaft, dismounting the machine, and mounting it again, is long, difficult, and expensive, to which one should add the economic loss caused by the lack of production from the machine. At worst, shaft failure could also represent a threat to the safety of the workers.

It is thus imperative to be able to foresee the failure of the shaft with a certain time margin. This could be achieved through traditional preventive maintenance: that is, by periodically inspecting the machine to make sure it is working properly, assessing that no significant damage has been undertaken by it (e.g. crack appearances, increase in clearances,…). The problem with this approach, as was stated by R. K. Mobley [5], is that it does not take into account the actual state of the machine before scheduling the maintenance, that is, it does not consider whether or not there is a need for maintenance, but only the time that has passed between sessions and the expected lifetime of the equipment. This will inevitably result in either unnecessary maintenance costs or a catastrophic failure.

The proposed alternative, which has gained a strong popularity over the past two decades thanks to the development of electronics, informatics, and the concept of industry 4.0, is predictive maintenance. Predictive maintenance consists on a regular (or constant) monitoring of the machinery through the use of a wide variety of sensors and other control instruments, allowing to schedule maintenance sessions only when the data shows the need for it, minimizing both failures and maintenance costs [5]. In line with this, the objective of this thesis is to build an on-line monitoring system for the eccentric press under study. This on-line monitoring system should have the ability to detect any deviation from the nominal working conditions and, ideally, schedule a maintenance session whenever it will be needed and give a preliminary diagnosis of what the cause of the problem might be.

1.1. Literature review

The research of the scientific literature was made using the scientific databases Scopus and ResearchGate, and the search engine Google Scholar. The documents considered were mainly books, journal papers, conference papers and literature reviews, although websites and white papers were also consulted occasionally. The objective of the literature review was to answer the following research questions [6]:

Q1 – What are the main variables involved in the hot forging process, how can they be measured, and how do they correlate with each other?

Q2 – What is the state of the art on monitoring and predictive maintenance of the hot forging process?

Q3 – How is vibration monitoring applied to predictive maintenance in general and to the hot forging process in particular?

For Q2, the research keywords used were ("forging" OR "eccentric press" OR "crank press") AND ("monitoring" OR "predictive maintenance" OR "control"). For Q1 a similar methodology was followed, with most of the keywords being specific of what was being searched. For example, for searching information regarding the measurement of temperatures, ("forging" OR "eccentric press" OR "crank press") AND ("temperature") AND ("thermocouple" OR "pyrometer" OR "thermo camera"). For Q3 the research focused more on vibration monitoring for fault detection and diagnosis in the manufacturing sector in general, and less on the hot forging process in particular, as there was not much information about it. Keywords ("vibration monitoring" OR "vibration analysis") OR ("predictive maintenance" AND ("vibration" OR "acceleration" OR "accelerometer")) were initially used, and then more were added as information was researched on specific topics of vibration monitoring.

Although no filtering was applied to the language in which the publications were written, only documents in English were used. Relevant articles were given priority over those with few citations, except for the newest ones or those exceptionally similar to the case being studied. The bibliographies of the most useful papers were also used as an important source of information.

1.2. Monitoring of the forging process

In order to design a predictive manufacturing system for the eccentric machine we first need to analyse the variables that are usually monitored in a forging process, how they are monitored, and how they correlate with each other.

First, the "reference variables" are time and/or ram position, and all the other variables will be studied as a function of one of those two. Time is already being recorded by sensors when they make their measurements, and ram position can be measured both through a linear displacement sensor (such as an incremental encoder, [7]), or through an optical encoder or a resolver [8][9] measuring the crank angular position. Measuring both time and ram position is especially relevant if the nominal angular speed of the shaft changes over time (which did not happen in the case under study). Other relevant variables that can be useful to monitor are:

- Ram velocity and acceleration.
- Weight, geometry, and temperature of the steel billet.
- Temperature of the dies.
- Forces involved in the process.

Ram velocity and acceleration can be obtained as the first and second derivatives of the ram position. The geometry of the billet is usually standardized and known a priori, and it should not show a relevant variance from one piece to another; while its weight can be measured with an electronic scale [10], and its temperature with an infrared pyrometer [10][11][12][13] (measuring it with thermocouples, while more accurate, would be unfeasible in an industrial context). Temperature of the dies can be measured with a combination of thermocouples inserted at different depths inside the dies [11][12][13][14][15]. The forces involved in the

process are mainly the forming force, but also the frame force and stopper force, which are usually measured with load cells made up of 4 strain gages forming a full Wheatstone bridge to compensate for thermal effects [10], [16]; and the ejector force, measured with a piezoelectric pressure sensor by measuring the pressure of the hydraulic ejector system [10].

The correlations between these variables during the forging process are studied in detail in [10], [17], [18], [19], [20], [21], [22], [15], [12], and [13]. On top of these, other alternative (or complementary) approaches include:

-The use of acoustic emission sensors: Doege et al. [10] state the usefulness of AE to detect cracks in the tool and in the workpiece, as advising for the positioning of the sensors as close to the metal forming process as possible to avoid noise disturbances (agreeing with Mukhopadhyay et al. [23]). The detection and diagnosis of failures using AE was achieved by El-Galy and Behrens [24], while Kong and Nahavandi [19] combined AE with force signals to predict tool wear, and Hawryluk et al. [25] integrated AE into a complex monitoring system for the hot forging process.

-The use of vibration monitoring through accelerometers: although it has not been extensively used for the monitoring of the forging process, there are some precedents of it, as will be discussed in the following section.

Some examples of fully integrated predictive maintenance systems can be seen in [8], [25], and [19].

1.3. Vibration monitoring

After considering the other possibilities presented in the previous section, it was decided to focus on the monitoring of the vibrations of the machine. This was done because of the convenience, simplicity, and efficiency of this method: vibrations analysis allows for a reliable monitoring of rotatory and reciprocating machines with only a few accelerometers [26], significantly reducing the costs and complexity with respect to the multi-sensors systems explained previously.

It is important to note that the monitoring of vibrations, as many other monitoring strategies in predictive maintenance, relies on 3 successive steps: detection of a fault, diagnosis (identifying the source of the problem), and prognosis (making an accurate estimation of the remaining useful life of working equipment, even after detecting and identifying a fault) [26]. Each step relies on the previous one being achieved and involves an increased level of complexity: as such, fault detection was the first objective of this work.

The scientific literature shows that an increase in clearances significantly increases the accelerations in a slider-crank mechanism like the one an eccentric press relies on [27][28][29], and, as it was previously explained, this is the main symptom found before shaft failure, so vibration monitoring should be adequate for detecting it. There are other cases in which vibration monitoring has been successfully applied to the forging process. Xu et al. [30] developed and experimentally tested a model of the vibration modes of a high-speed servo numerically controlled punching press. Glaeser et al. [31] noticed the need for part classification to predict tool wear through the monitorization of vibrations in cold forging, and successfully achieved it. Their research was later continued [32] and they were able to detect and classify different kind of faults with the application of different deep learning algorithms.

1.4. Signal processing and features selection

As it was explained in section 1.3, fault detection was the first objective of this work. To do this it was necessary to identify a range of nominal values on a set of features of the acquired data, both on the time and frequency domain, if possible. The features used to achieve this were:

-Time domain: the different features used can be seen in Table 1. It was found by Glaeser et al. [32] that RMS was the most important feature to detect faults in a cold forging system, and all faults were accompanied by an increase in the RMS levels of the recorded vibrations. Caesarendra et al. [33] indicate how the RMS increases gradually as faults develop in rolling element bearings, and it is the feature used in ISO standards 10816 to measure the acceptable levels of vibrations for acceleration, velocity and displacement [34]. Crest factor, kurtosis, and skewness are also common features for monitoring accelerations in the time domain [32], so they were used too.

Feature	Formula
RMS	$\sqrt{\frac{1}{N}\sum_{i=1}^{N} x_i^2}$
Crest-factor	$\frac{max\|x\|}{\sqrt{\frac{1}{N}\sum_{i=1}^{N} x_i^2}}$
Skewness	$\frac{\sum_{i=1}^{N}(x_i - \mu)^3}{(N-1)\sigma^3}$
Kurtosis	$\frac{\sum_{i=1}^{N}(x_i - \mu)^4}{(N-1)\sigma^4}$

Table 1. Features used for time domain monitoring, with N being the number of values taken by the discrete variable x, μ being the average of x, and σ being its standard deviation.

The envelope of the signal was studied too, as it is considered one of the most powerful tools for fault detection and diagnosis in vibration monitoring [35]. Although it is mainly applied to rolling bearings monitoring, it was found by Shen and Ai [36] that the shape of the envelope of the forging force and the vibrations generated by it can be monitored to detect faults in the forging process.

-Frequency domain: the power spectrum is used to characterize the frequency response of the machine by calculating several features such as the Frequency Centre (FC), the Root Mean Square Frequency (RMSF), and the Root Variance Frequency (RVF). FC and RMSF show the position centres of main frequencies, while RVF describes the convergence of the power spectrum towards the frequency centre. A fault in the machine is expected to change the frequency domain of the vibrations, which would also cause a change in FC, RMSF, and RVF [33][37]. The formulas for calculating each of these features are shown in Table 2.

Feature	Formula
FC	$\frac{\int_0^\infty f\, s(f) df}{\int_0^\infty s(f) df}$
RMSF	$\sqrt{\frac{\int_0^\infty f^2 s(f) df}{\int_0^\infty s(f) df}}$
RVF	$\sqrt{\frac{\int_0^\infty (f - FC)^2 s(f) df}{\int_0^\infty s(f) df}}$

Table 2. Features used for frequency domain monitoring, where f is the frequency and s(f) is the power spectrum at frequency f.

-Time-frequency domain: as FFT based methods have been found inadequate for non-stationary signal analysis [37], it was decided to use a tool better suited for studying said type of signals. The Short Time Fourier Transform (STFT) was chosen for this, as it is considered an effective way of analysing non-stationary signals in general [33][37], and has been proved adequate to monitor the forging process, as Glaeser et al used it (alone with wavelet) for part classification in cold forging [31].

1.5. Document organisation

The remaining content of this work has been organised in the following sections: proposed method (section 2), results (section 3), discussion (section 4), and conclusions (section 5). Section 2 presents the experimental setup for data acquisition that was used, as well as the methodology followed in the analysis of the measurements. In section 3 the results obtained from applying the methodology are shown. Section 4 is devoted to explaining and commenting the results. Finally, section 5 indicates the future investigations that could be done to continue this work, as well as giving the final considerations on the achieved results.

2. Proposed method

2.1. Experimental setup

It was decided to use piezoelectric accelerometers, as they are by far the most used sensors for vibration monitoring in industrial applications [5][32][26][38]. A total of 6 sensors were used: 2 of them (model Dytran 3225F1T) with a sensitivity of 10 mV/g (designated as A4 and A5), and the other 4 (model Brüel & Kjaer 4526) with a sensitivity of 100 mV/g (A0 to A3). All of them were able to measure accelerations up to 510 m/s^2, and had a sampling frequency of 1652 Hz, allowing for the monitorization of vibrations up to 826 Hz. Signals were acquired through a NI 9234 data acquisition board by National Instruments (Austin, Texas).

The eccentric mechanical press being studied is a slow system involving very big masses, so the monitoring of frequencies above 1kHz was not considered necessary. It is common to use much higher sampling frequencies in some vibration monitoring applications (in the order of tenths of kHz), especially when trying to detect faults in bearings in specific frequency ranges. However, this is usually done when said frequency ranges are known, which is usually achieved by monitoring both a "regular" machine and one with a known defect created solely for this purpose [5], and this was not possible in this case. It was stated by Salahshoor et al. [29] that a slider-crank mechanism with no defects would show peaks ranging from 1X to 5X times its rotational frequency when analysing its vibrations in the frequency domain (without taking into account its natural frequency). The press under study is working at just 1500 rpm (25Hz), so the chosen sampling frequency was considered high enough. Agreeing with this, Lacey [39] indicates that frequency ranges as narrow as 10-1000 Hz can be adequate for monitoring the overall vibration level with the intent of detecting

defects in rotating machines, and Glaeser et al. [31] achieved part classification in a cold forging process using an accelerometer with a sampling frequency of 1650 Hz.

Regarding sensors location, it is common practice to either position accelerometers in 3 perpendicular axes in order to be able to measure accelerations in all of the 3 dimensions [27], or to use 3-axis accelerometers [9][31]. While acoustic emission signals suffer severe attenuation and distortion due to their high frequencies (at least in the order of hundreds of kHz), and thus require sensors to be mounted as close to the process as possible, regular vibration monitoring is not affected by this, as it measures vibrations in much lower frequencies, allowing for the mounting of sensors relatively far away from the process itself [40].

As some of the previously mentioned publications study the effects of clearances on the coupler or the slider of a slider-crank mechanism [28][29], it might have been interesting to position the accelerometers in the ram or the coupler of the press in order to replicate those results. However, mounting the sensors in the moving parts of the press would have considerably increased the complexity of the setup (as well as the risk of damaging the sensors during the press operation), so it was chosen to mount them in the press frame, as can be seen in Figure 5.

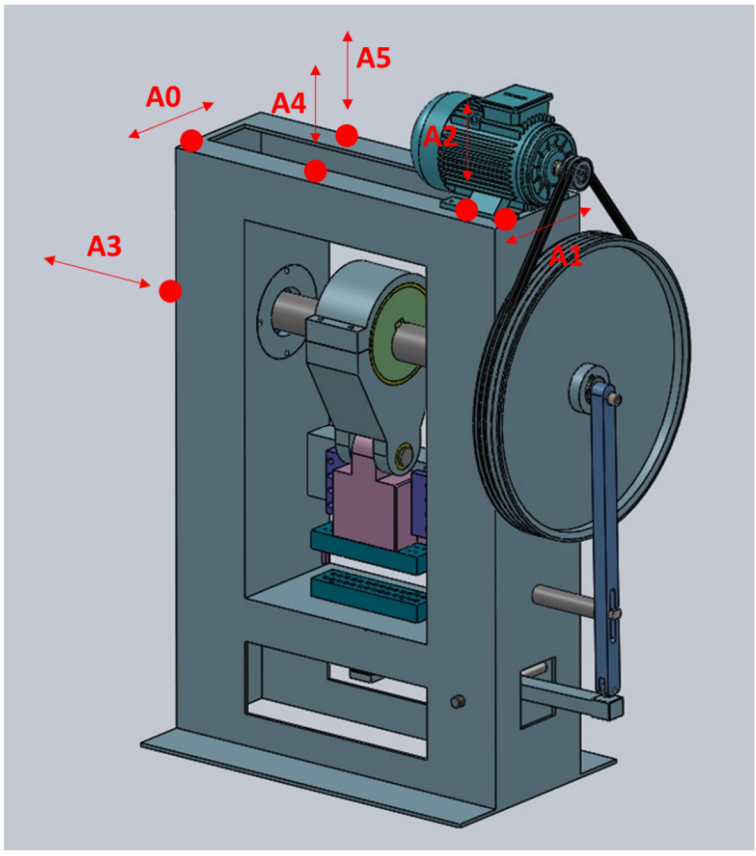

Figure 5. Sensors location [2]

2.2. Signal processing

After a first step of importing the measurements from the original .tdms files and storing them in a single .mat file, the data was reorganized in several matrices (section 2.2.1), a set of different frequency filters were applied (section 2.2.2), and the envelope of curves was calculated (section 2.2.3). All the calculations and graphs were done using the software MATLAB®.

2.2.1.Identification of groups, hits, and parts

Once the measurements were stored in a single matrix it was needed to reorganize the data in order to be able to work with it. To do this, four cell arrays were created. The first two contained the indexes of the beginning and end of each 3-hits group (one for each stage of the machine) and each hit respectively, both referred to the original matrix of data. The third contained the acceleration measurements of each individual hit, and the fourth contained the indexes of the beginning and end of each part of each hit referred to the third cell array. The use of indexes was chosen because of storage reasons: the original matrix containing all data was too big (6 GB), so duplication of information was avoided as much as possible to find a compromise between storage efficiency and convenience.

Three different algorithms were developed for the identification of 3-hits groups, hits, and parts of hits. The first two used a moving time window and an acceleration threshold to allow the code to differentiate the noise from the useful measurements. The moving windows had a length of 5 seconds for the groups identifier algorithm, and 0.5 for the hits identifier. The acceleration thresholds were defined as a multiple of the RMS of the measurement being analysed, with 5*RMS being the threshold for the groups identifier, and 1*RMS for the hits identifier. The beginning of each group (or hit) was found when a point above the threshold entered the moving window if there were none in the previous time instant. The end was found when there was only one point above the threshold inside the window, and there were none in the next time instant. An example can be seen in Figure 6 for 3-hits groups identification.

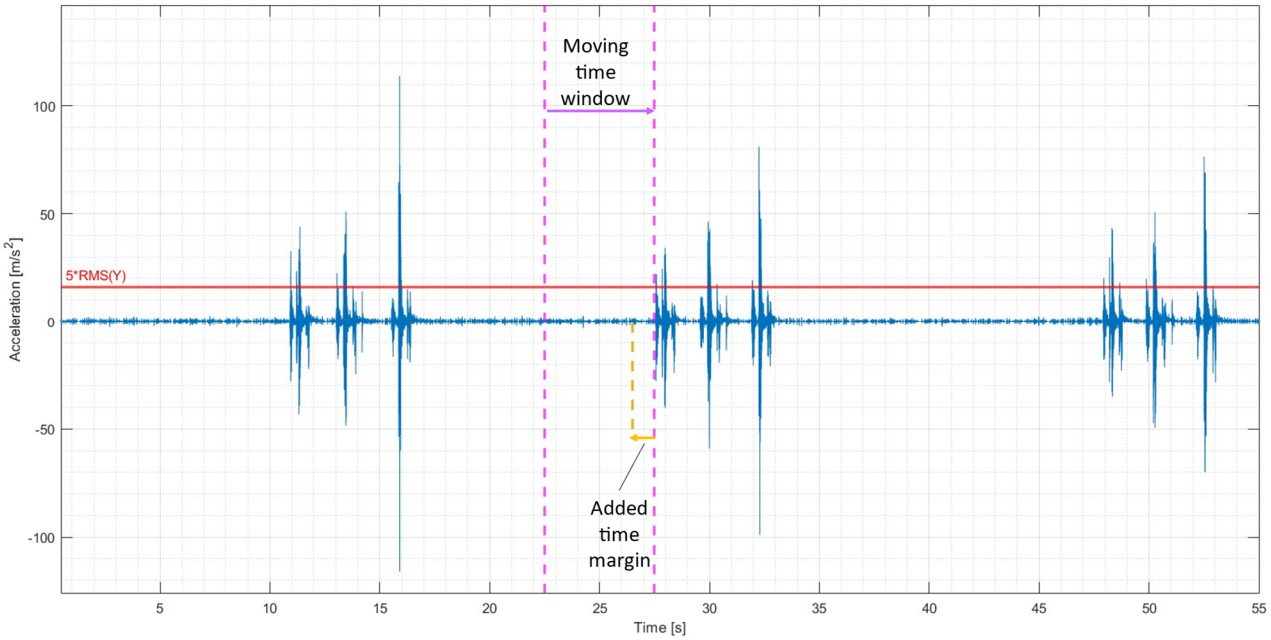

Figure 6. Identification of the beginning of a 3-hits group

This approach was not adequate for identifying the parts of each hit: the big variability found made it impossible to set a threshold and a window length that would work for all measurements. Attempts at doing so resulted either in some parts not being detected, or too many part divisions found were there should have been none. Because of this, the part identification was done by finding the valleys of the integral of the absolute value of the acceleration over a moving time window of 0.075 seconds, as can be seen in Figure 7. In order to eliminate excessive relative minimums, the curve of the integral was smoothed with a moving average of 30 elements. The detection of the valleys in the middle of parts 2 and 3 was avoided by requiring a minimum time width between valleys for them to be considered as part separations. This minimum width was 5% of the time length of the overall hit. The position of the valleys in the time domain was slightly moved forward in time by 0.035 seconds to compensate for the delay between the curve of the integral and that of the real hit.

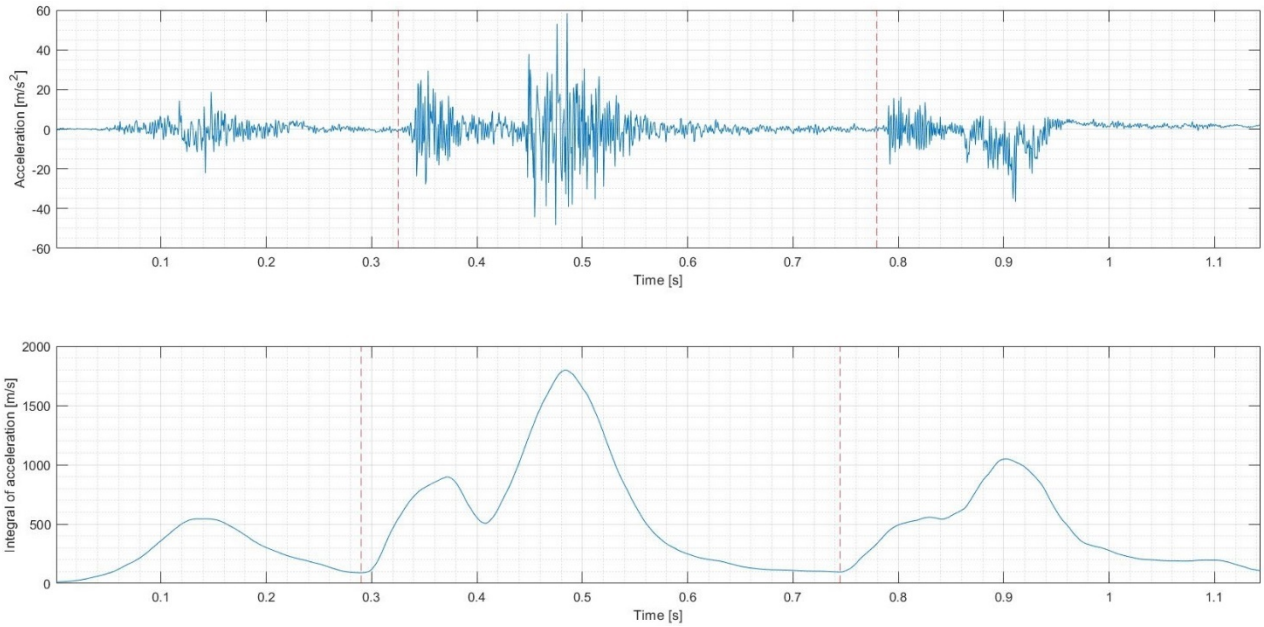

Figure 7. Integral of the absolute value (below) used to identify parts of a first hit measured by A0 (above)

In the first method small time margins were added before the beginning and after the end to make sure no information was lost because of a possible lack of precision of the algorithm. These were 1 second for groups identification, and 0.1 seconds before the beginning and 0.2 after the end for hits identification. A minimum time length of 5 seconds was required for 3-hits groups to be considered valid, as at some points during the day the press had performed setup operations, and there were measurements that could not be considered nominal conditions. 3-hits groups that were split between different .tdms files were not considered. Even after this filtering of outliers most of the groups, hits and parts could be correctly identified, resulting in 769 3-hits groups, which were considered enough to characterize the nominal conditions of the machine.

2.2.2. Frequency filtering

Once the data was reorganized, several frequency filters were applied. Four Butterworth filters were used:

- A low-pass filter of order 25 with a passband frequency of 200 Hz, a stopband frequency of 250 Hz and a cut-off frequency of 204 Hz.
- A low-pass filter of order 35 with a passband frequency of 300 Hz, a stopband frequency of 350 Hz and a cut-off frequency of 305 Hz.
- A high-pass filter of order 38 with a passband frequency of 300 Hz, a stopband frequency of 250 Hz and a cut-off frequency of 296 Hz.
- A high-pass filter of order 37 with a passband frequency of 500 Hz, a stopband frequency of 450 Hz and a cut-off frequency of 495 Hz.

The order of the filters and the exact cut-off frequencies were chosen so that they would have a maximum ripple in the passband of 1 dB and a minimum attenuation in the stopband of 60 dB.

2.2.3. Envelope calculation

As stated in section 1.4, the shape of the envelope can be a useful tool for characterizing the nominal conditions of the machine. The envelope of the curves was calculated using the MATLAB® function envelope(), which calculates it as the magnitude of the analytic signal of the original curve. Both the upper and lower envelope were obtained for each part of each hit of each sensor, and it was computed for the raw signal and for each of the filtering conditions explained in section 2.2.2. The procedure for studying its shape is explained in section 2.3.1, and the results are presented in section 3.2.1.

2.3. Feature extraction and analysis

The features in the time domain and frequency domain presented in section 1.4 were calculated for all measurements of all conditions. In this work, the "condition" is defined as a measurement:

- Taken by the same sensor
- Of the same hit (first, second, or third)
- Of the same part of the hit (see section 3.1)
- Applying the same frequency filter (see section 2.2.2.)

It is worth noting that, when considering the frequency filters, the condition of no filtering was also studied. In a similar way, when considering the part of the hit, the features obtained from analysing the whole hit were also taken into consideration. This was done to decide whether it was useful for the monitoring of all features to apply frequency filters or to divide the hits into their different parts. The mean value and other features that involve it (like shape factor or standard deviation) were not considered, as the mean accelerations were 0.

The main objectives of this process were:

- To set an upper and lower threshold for the most reliable features, so non-nominal conditions could be detected if future measurements were to be outside those bounds.
- To identify the most important sensors to monitor, so that the number of accelerometers could be reduced to lower the costs of the monitoring system.

The intervals made by the upper and lower thresholds were calculated as μ (mean) $\pm 2\sigma$ (standard deviation) for each feature in each condition, using all 769 measurements. These bound were used to calculate the percentages of measurements contained within their respective intervals (Table 3 and Table 4), but these percentages were also tested with the bootstrap sampling method. This process worked as follows:

- 30% of the measurements of a given condition were used to calculate an interval for a given feature.
- The percentage of measurements (from the remaining 70%) that were contained within the intervals was calculated, and that value was stored.
- The process was repeated 5000 times.
- The distribution of percentages was studied.

Only "narrow" intervals were considered useful, which were defined as those in which the ratio σ/μ was smaller than 25%, and preferably lower than 15%. The σ/μ ratio is known as the Coefficient of Variation (CV), and, as it is a relative indicator, can be used as a measure of variability to compare non-negative samples with different units or very different mean values [41].

The results obtained from this procedure can be seen in section 3.2 for the time domain, and section 3.3 for the frequency domain.

2.3.1. Envelope analysis

The shape of the envelope was analysed using the cross-correlation function. This was done in two steps:

- First step

The idea behind this first step was to know how similar the shapes of the envelopes of signals of the same condition of a given part of the hit were among each other, and how different they were from envelopes of different conditions of that same part. The similarities in shape were measured through the cross-correlation, but the cross-correlation function can only compare two curves at the same time, so there was no way to directly compare all curves simultaneously. Because of this, an algorithm was developed to compare a lot of pairs of curves at the same time. The number of pairs of curves compared had to be big enough to give the results statistical significance. As there were 769 curves of each condition, it was chosen to make 5000 pair comparisons for each condition.

The algorithm used works as follows. First a reference condition is chosen (sensor, hit (first to third), part of the hit, and filtering, if any). The cross correlation between the envelopes of 2 random curves of this condition is calculated, using the necessary time lag between curves to achieve the maximum cross correlation possible (this is easily done with the MATLAB® function xcorr()). The value is stored and the process is repeated a high number of times (in this case, 5000 iterations), resulting in a distribution of values. A block diagram showing this process can be seen in Figure 8.

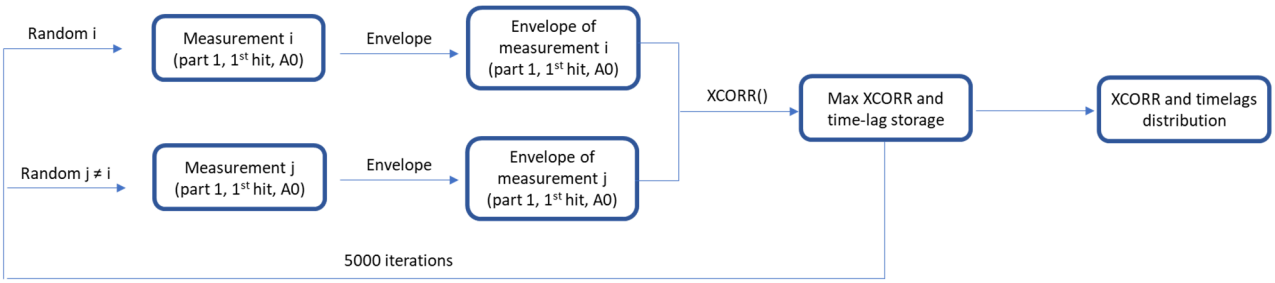

Figure 8. Example of envelope cross-correlation analysis for the reference condition of first hit, clutch part of the hit, measured by A0, with no frequency filters.

The whole process is repeated several times, now calculating the maximum cross-correlation between a curve of the reference condition and another of a different one (different sensor and/or hit, but same part of the hit and filtering conditions). This results in 15 distributions of data (5 useful sensors multiplied by 3 different hits), in which the distribution corresponding only to pairs of curves of the reference condition is expected to reach clearly higher values than the others. These 15 distributions of data can be compared against each other using box plots, allowing to visualize the influence of sensor and hit regarding the similarity between the shape of the envelopes. The normalized cross correlation is the one being used (between 0 and 1) to allow for an easier comparison between calculations. The process is studied both for the upper and lower envelope..

- Second step

The ultimate objective would be to find a way to monitor the shape of the envelope and identify non-nominal working conditions through a change in its shape. To do this some kind of "standard" envelope curve would be needed so new measurements could be compared against them. Those standard curves were created for each condition by first calculating the envelope curves of all measurements of said condition, and then picking the median value for each time instant, in a similar procedure to the one used by Shen and Ai [36]. These curves were tested by calculating the maximum cross-correlation with the envelopes of all measurements of the same condition, and those of the same part and filter but different sensor and/or hit.

2.3.2. STFT

The STFT was not analysed as a feature, but only used to help understanding the behaviour of the data both in the time and frequency domain, and to test or validate the conclusions drawn from the other methods. It was calculated using time intervals of 50 points, that is, 30.27 milliseconds (sampling frequency being 1652 Hz).

3. Results

3.1. Time domain data

The press was continuously monitored for 30 hours using the accelerometers setup previously described and the data was stored in several .tdms files, each containing 5 minutes of measurements for each sensor. The resulting data consisted in 350 files for each sensor, like the one in Figure 9.

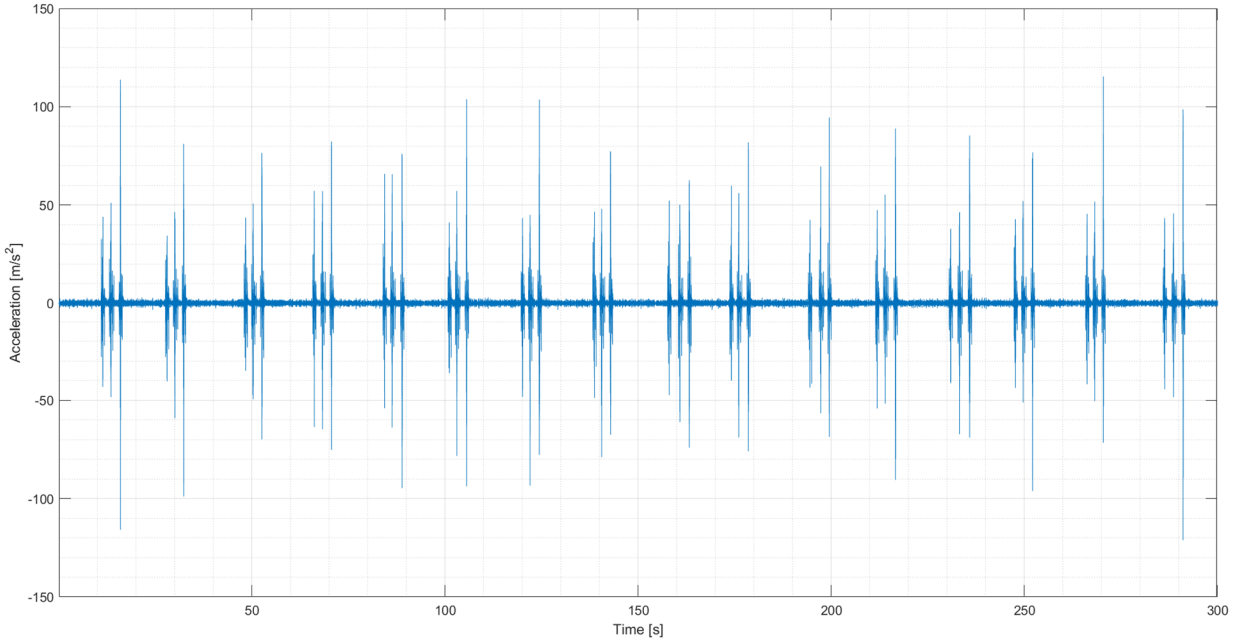

Figure 9. Example of measurement taken by A0

Figure 10 and Figure 11 show the variation on the number of 3-hits groups per measurement, and thus on the productivity of the machine.

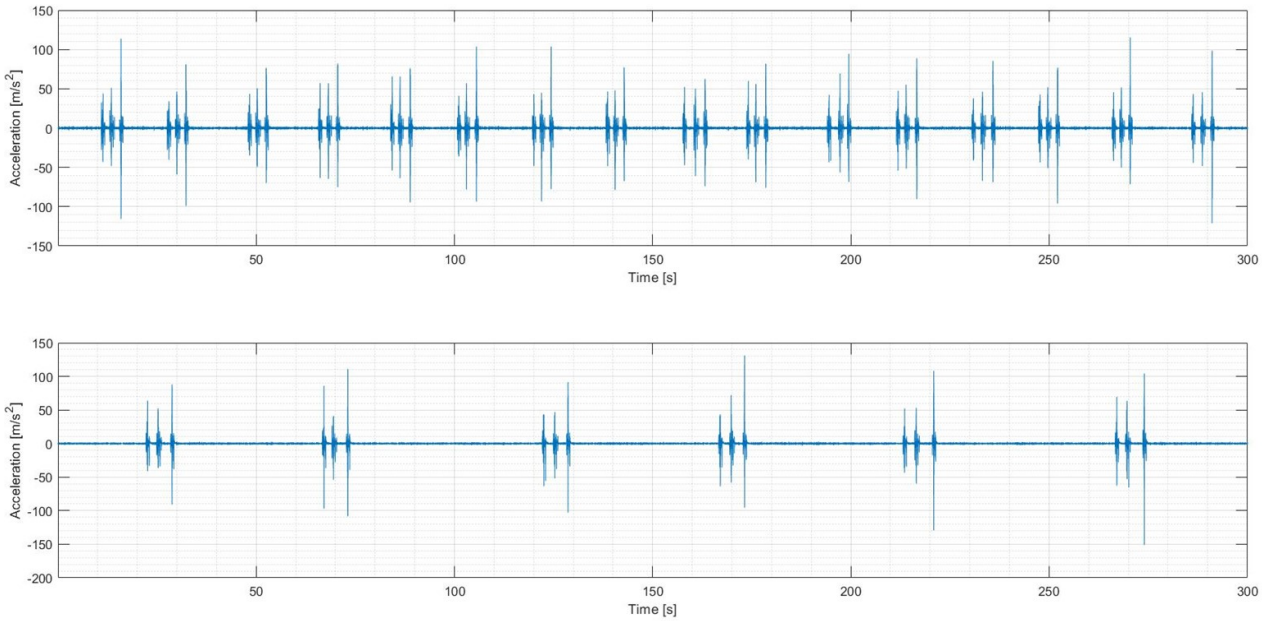

Figure 10. Example of the variation on the number of 3-hits groups between two different measurements

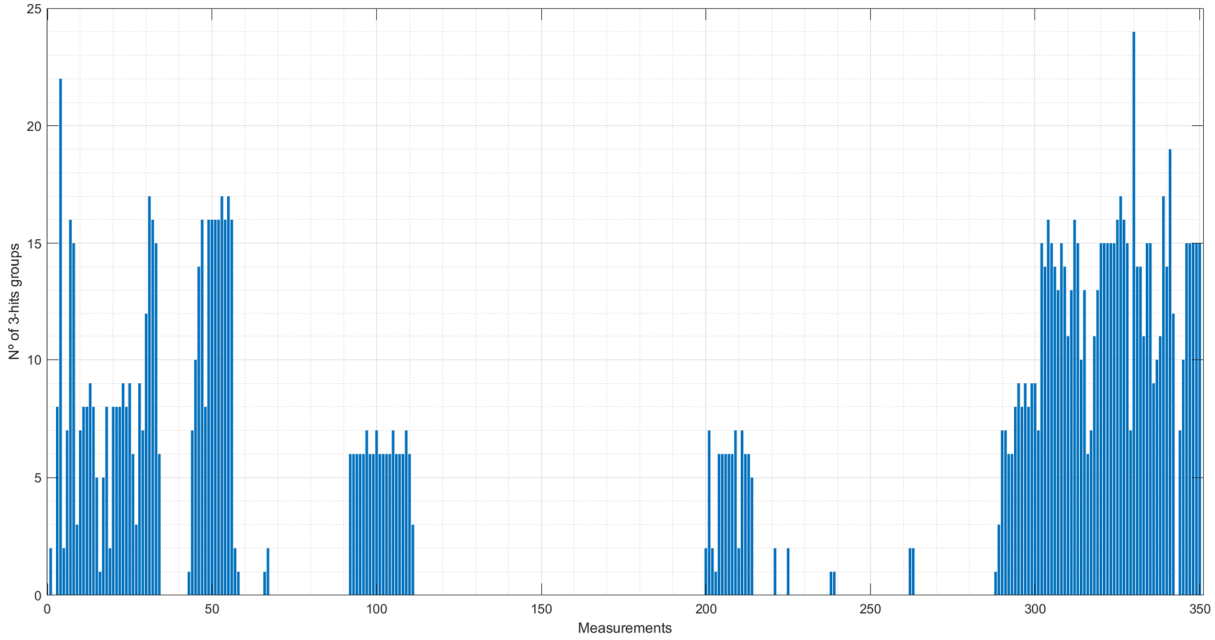

Figure 11. Variation on the number of 3-hits groups through the measurements

Inside each hit 3 separated parts were identified, which can be seen in Figure 12. The first part will be referred to as "clutch part", the second as "forging part", and the third as "brake part", according to the main causes behind each of them (explained in section 4.1) A fourth part was found only on the second hit, corresponding to the second stage of the press.

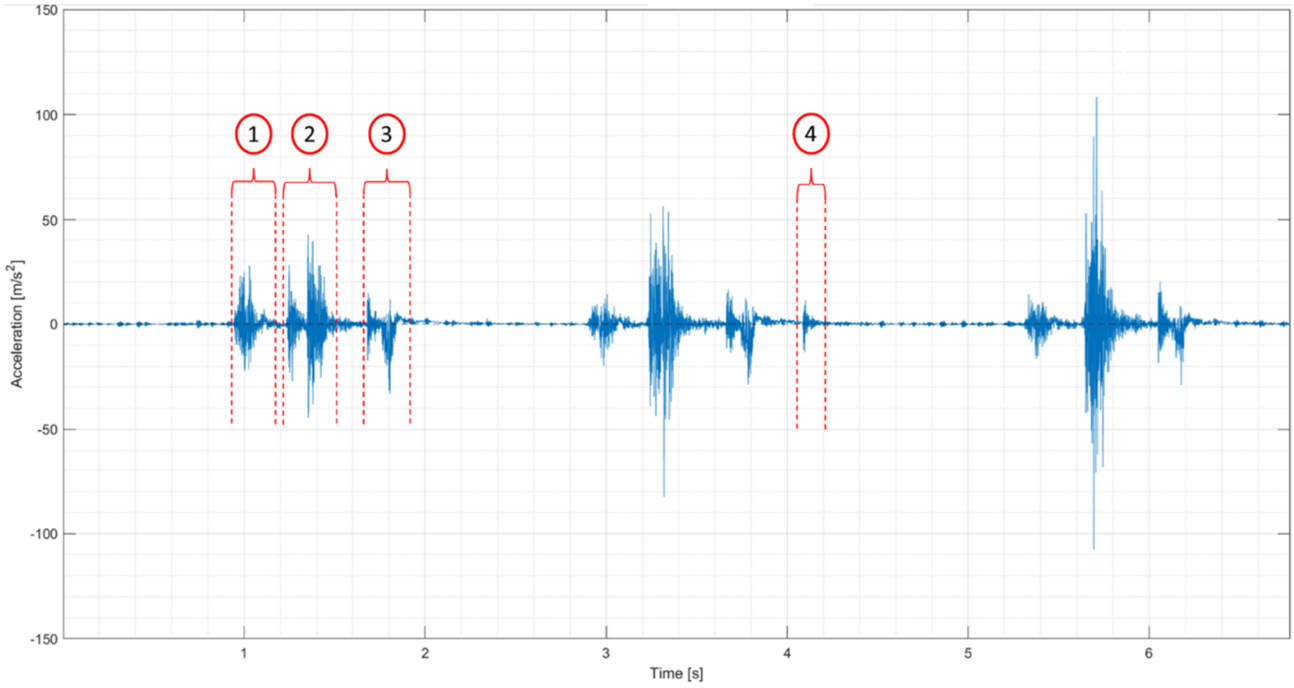

Figure 12. Zoomed example of a 3-hits group measured by A0

The forging part is divided in 2 halves in the first hit, while the division is less clear but still present in the second hit, and not present at all in the third hit (Figure 13).

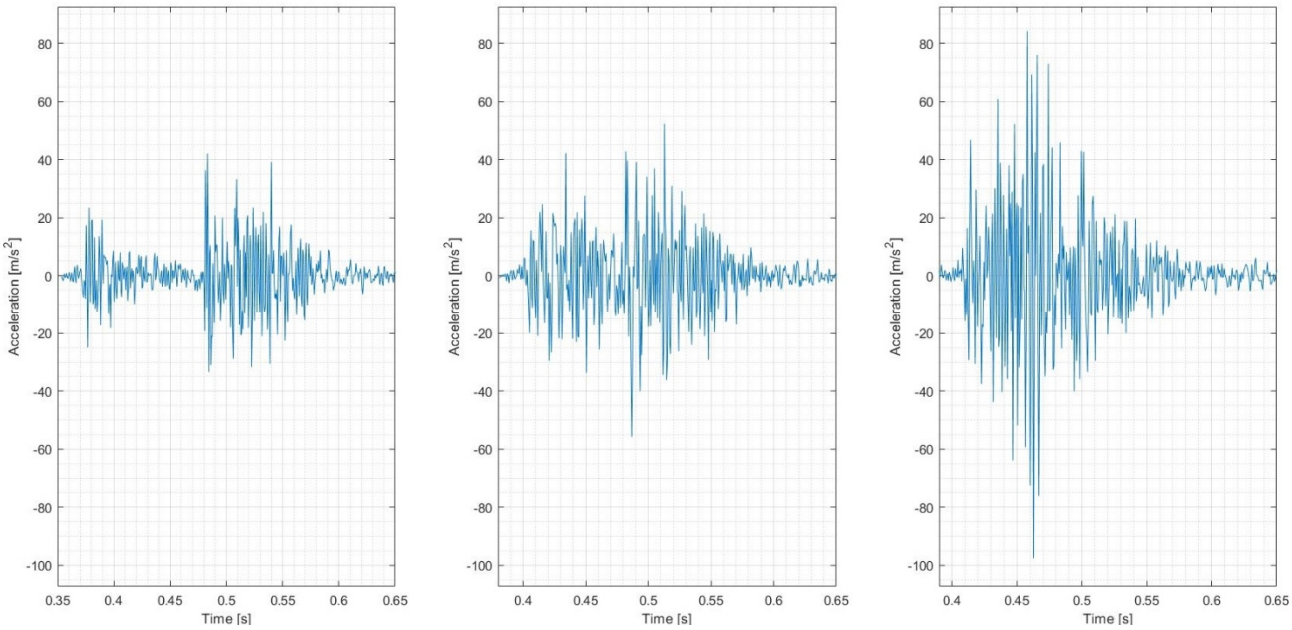

Figure 13. Example of the forging part of the hit (from left to right, first, second, and third hit) measured by A0

The brake part was also divided in two halves (Figure 14). Sensors A0 and A1 show that the second half is not centred in 0, while sensors A2, A4 and A5 do not show this. The second half of the brake part was dominated by low-frequency components, while the first half is dominated by higher frequencies (Figure 15 and Figure 16). The same, but to a lesser extent, occurs when looking at the clutch part of the hit (Figure 17).

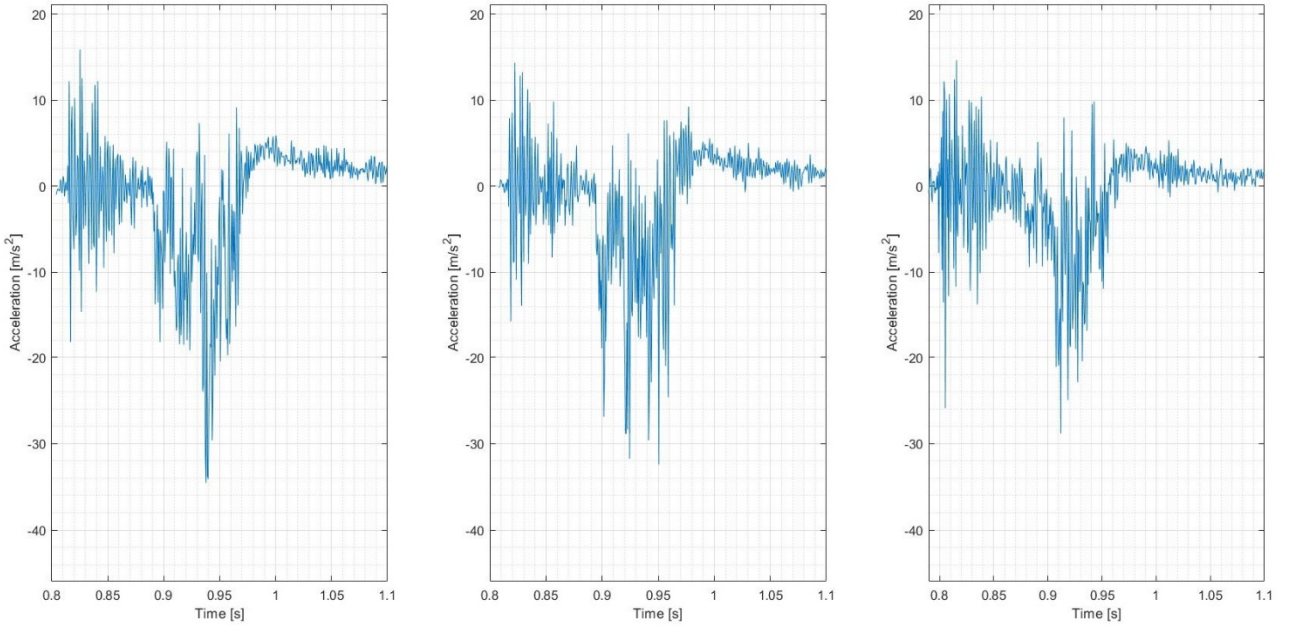

Figure 14. Example of the brake part of the hit (from left to right, first, second, and third hit) measured by A0

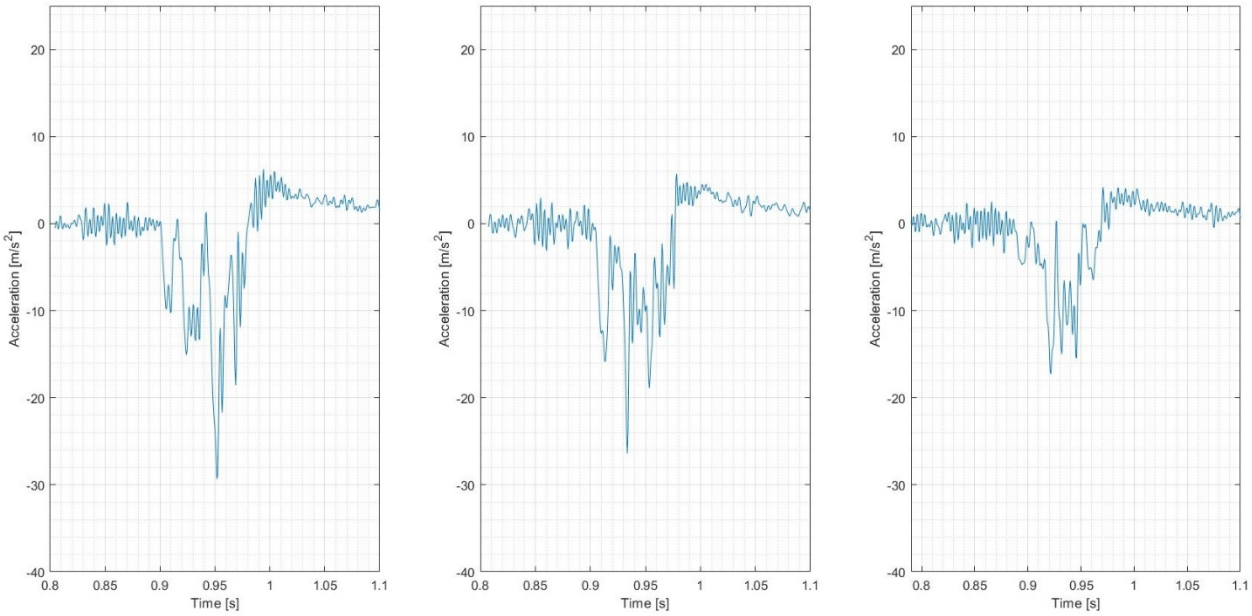

Figure 15. Example of the brake part of the hit (from left to right, first, second, and third hit) measured by A0 after applying a low-pass filter of 300 Hz

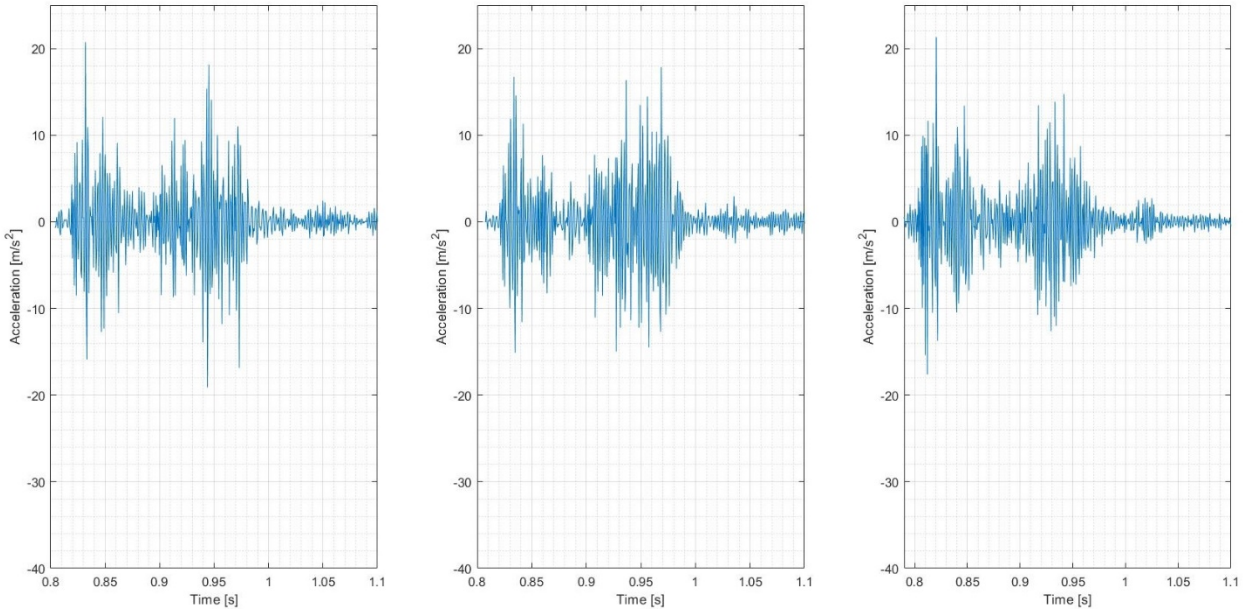

Figure 16. Example of the brake part of the hit (from left to right, first, second, and third hit) measured by A0 after applying a high-pass filter of 300 Hz

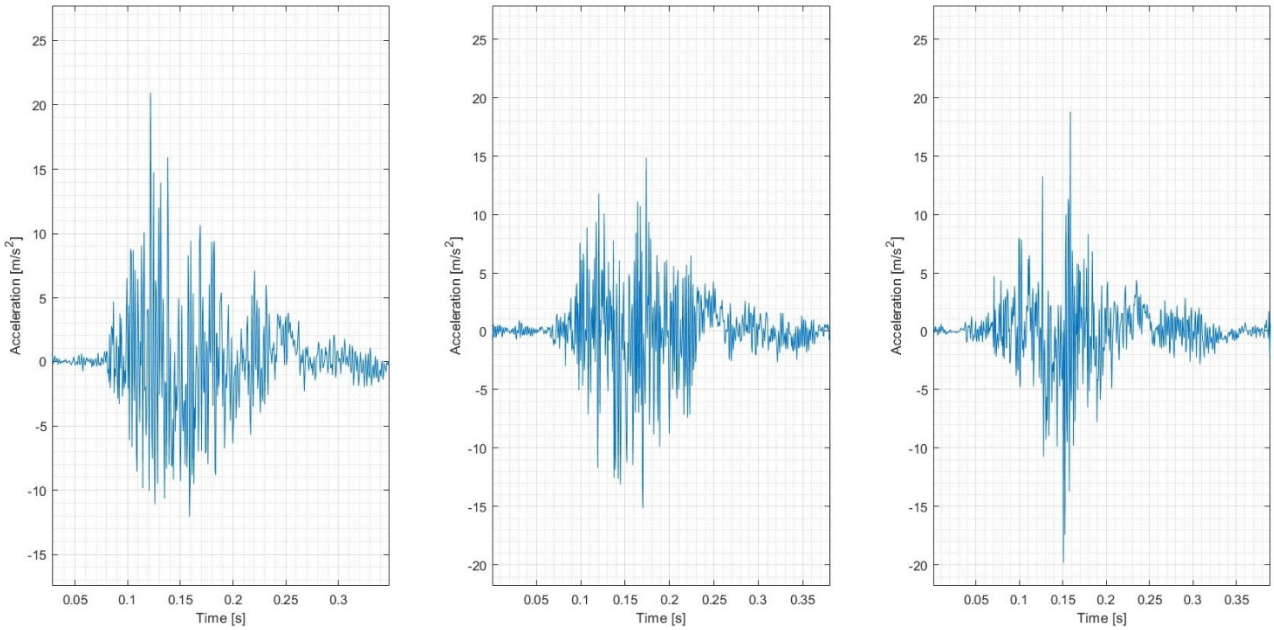

Figure 17. Example of the clutch part of the hit (from left to right, first, second, and third hit) measured by A0

3.2. Features in the time domain

A confidence interval of μ (mean) ± 2σ (standard deviation) was created for each feature in each condition, and it was found that more than 90% of the measurements were contained inside their corresponding interval. These percentages always remained above 90% when applying the bootstrap sampling method described in section 2.3. This is higher than the theoretical minimum established by Chebyshev's inequality, which states that at least 75% of the values of a dataset are contained within the interval μ ± 2σ, but it is still lower than the 95% minimum for normal distributions. The exact results can be seen in Table 3, and two examples of confidence intervals for the RMS can be seen in Figure 18 and Figure 19. Normality tests were performed on the data, but it was concluded that they could not be modelled as normal distributions.

	RMS	**Crest Factor**	**Skewness**	**Kurtosis**
Minimum	94.29%	94.03%	92.99%	93.24%
Maximum	100.00%	98.05%	99.35%	98.44%
Mean	96.32%	95.77%	95.24%	95.75%
Median	95.97%	95.71%	95.06%	95.71%
Standard deviation	1.34%	0.65%	0.91%	0.79%

Table 3. Statistics of the percentage of measurements' time-domain features contained between μ ± 2σ

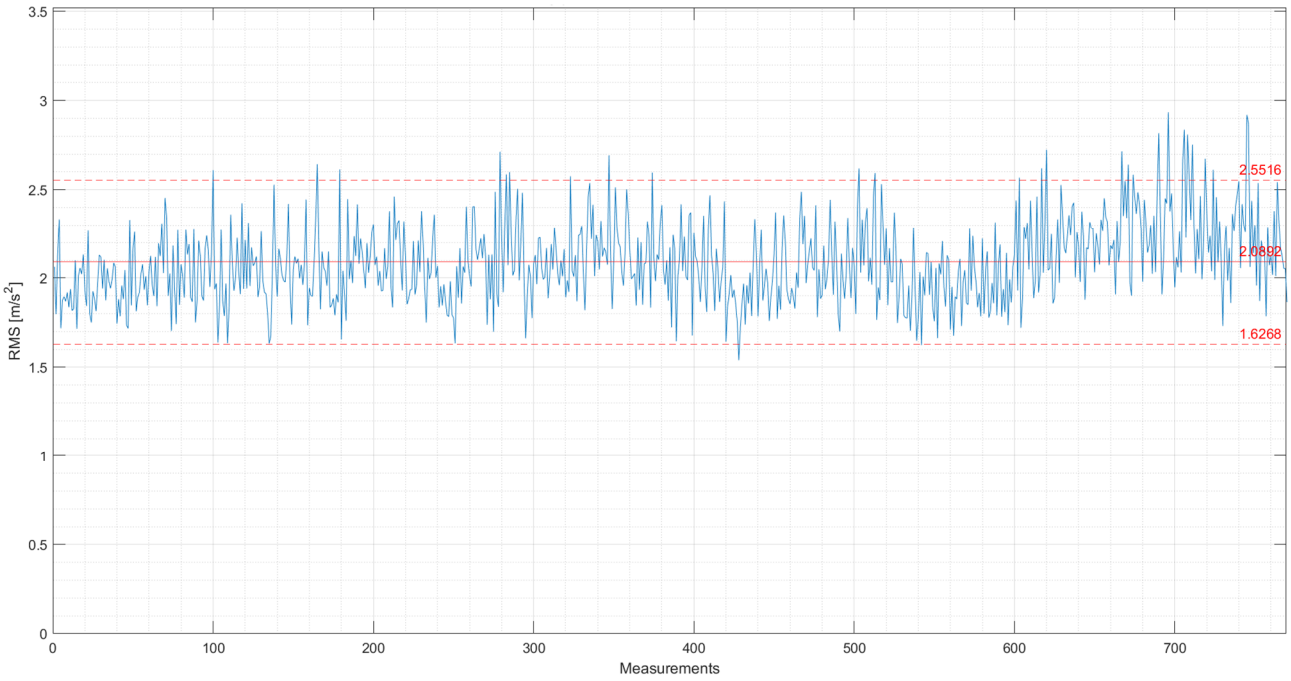

Figure 18. Example of a confidence interval for the RMS of the clutch part of the hit measured by A0 applying a low-pass filter of 300 Hz

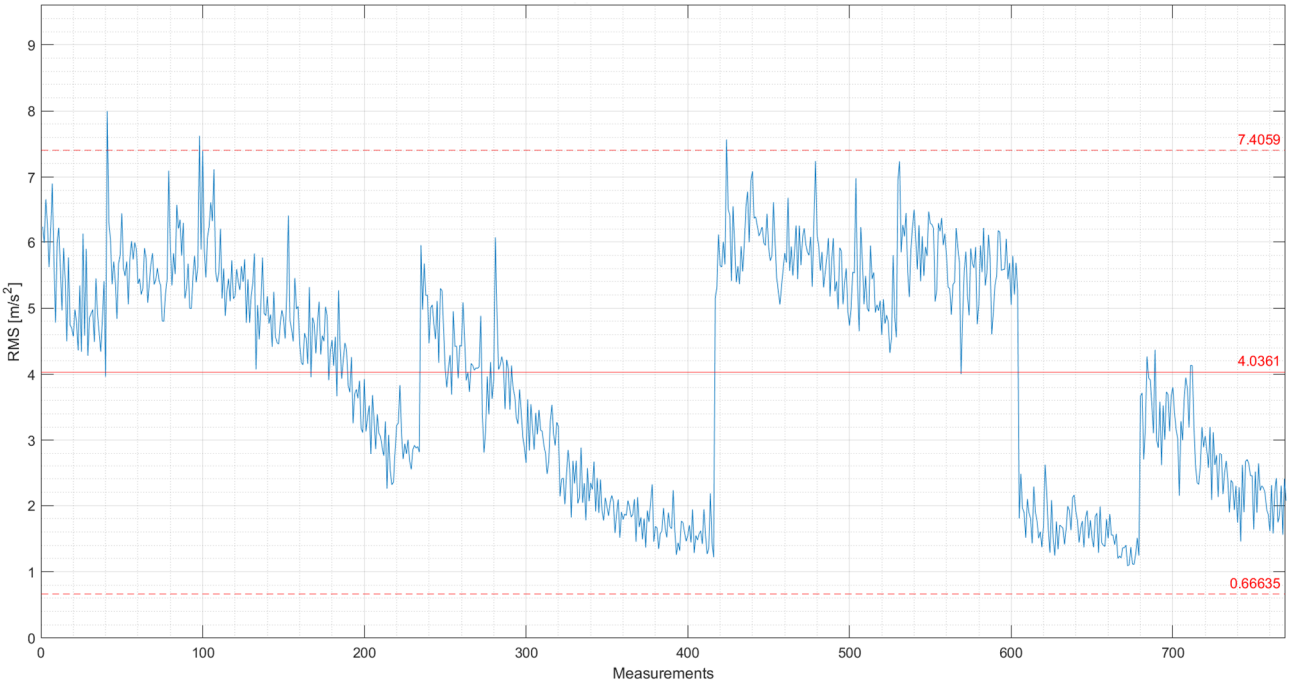

Figure 19. RMS of the time series of the brake part of the hit measured by A1 applying a low-pass filter of 300Hz

RMS showed σ/μ<25% for all sensors when monitoring the clutch part of the hit, and this ratio was especially low when considering low-pass filters applied to sensors A0, A1 and A2 (between 8% and 13%). The same occurred when monitoring the RMS of the forging part of the hit: σ/μ ratios were consistently under 15% for all sensors when no filtering was applied, and they were almost equally low when considering the different frequency filters, always remaining under 25%. RMS of the brake part of the hit showed σ/μ<25%, and mostly <15%, for all conditions except no-filtering and low-pass filters applied to A0 and A1 (Figure 20).

Crest factor showed low σ/μ ratios (<20%) for all conditions, with low pass filters showing the lowest ratios. Figure 20 and Figure 21 show the values of σ/μ obtained for RMS and crest factor for the brake part, with each row indicating a different frequency filter, each column a different combination of measuring sensor and hit, and color green indicating σ/μ<15%, yellow 15%<σ/μ<25%, and red σ/μ>25%.

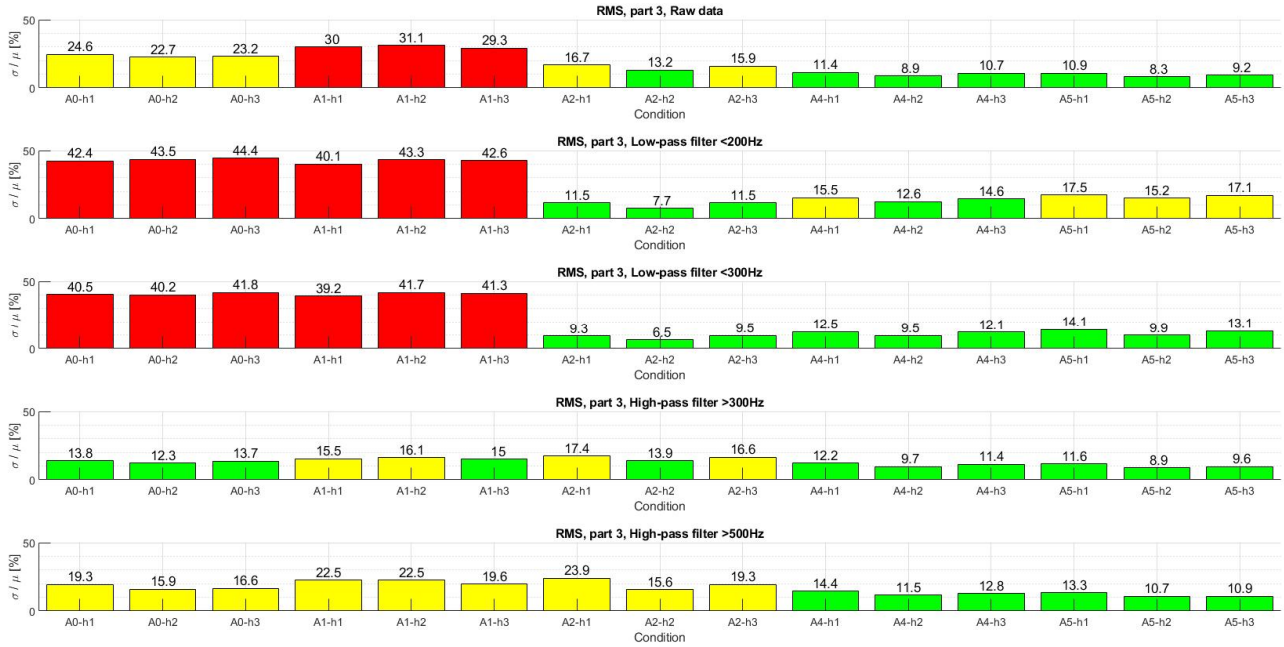

Figure 20. σ/μ ratios for RMS in the brake part of the hit

Figure 21. σ/μ ratios for crest factor in the brake part of the hit

The σ/μ ratio cannot be used to study kurtosis and skewness, as these variables can take non-positive values. However, it was found that all conditions had positive lower bounds for kurtosis. Measurements were not clearly skewed in a positive or negative direction for any condition.

3.2.1. Envelope analysis

As explained in section 2.3.1, the analysis of the shape of the envelope was performed in two steps. In the first step the highest cross-correlations were found when using the lower envelope calculated after applying a low-pass filter of 200 Hz. Figure 22, Figure 23 and Figure 24 show some of the results obtained.

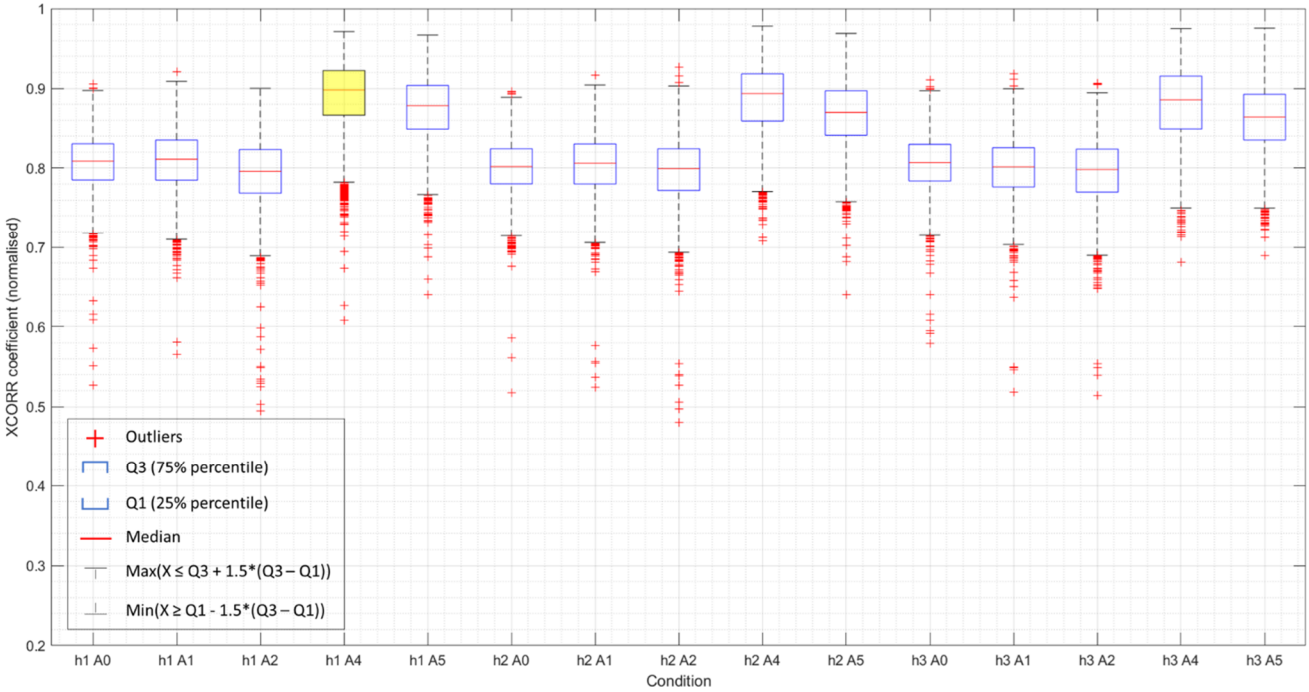

Figure 22. Cross correlation of lower envelope curves of the clutch part of the hit after applying a low-pass filter of 200Hz. Hit 1 measured by A4 (h1 A4) is the reference condition, indicated by the yellow box.

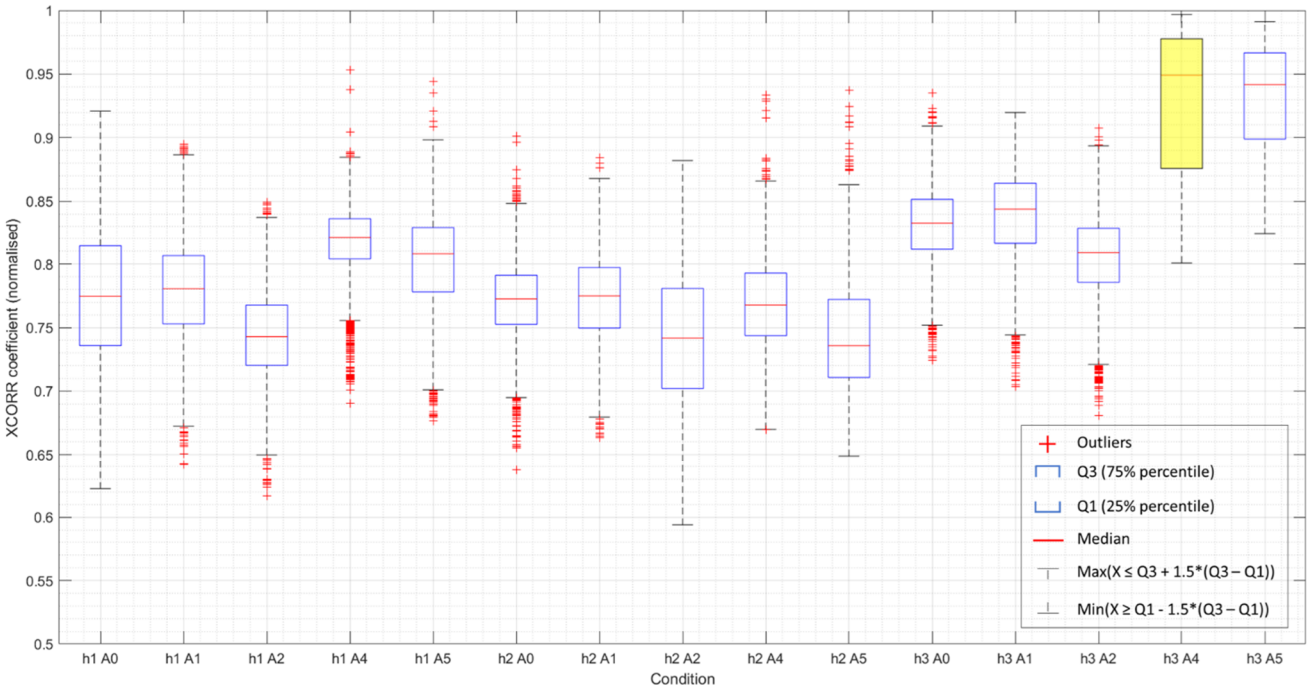

Figure 23. Cross correlation of lower envelope curves of the forging part of the hit after applying a low-pass filter of 200Hz. Hit 3 measured by A4 (h3 A4) is the reference condition, indicated by the yellow box.

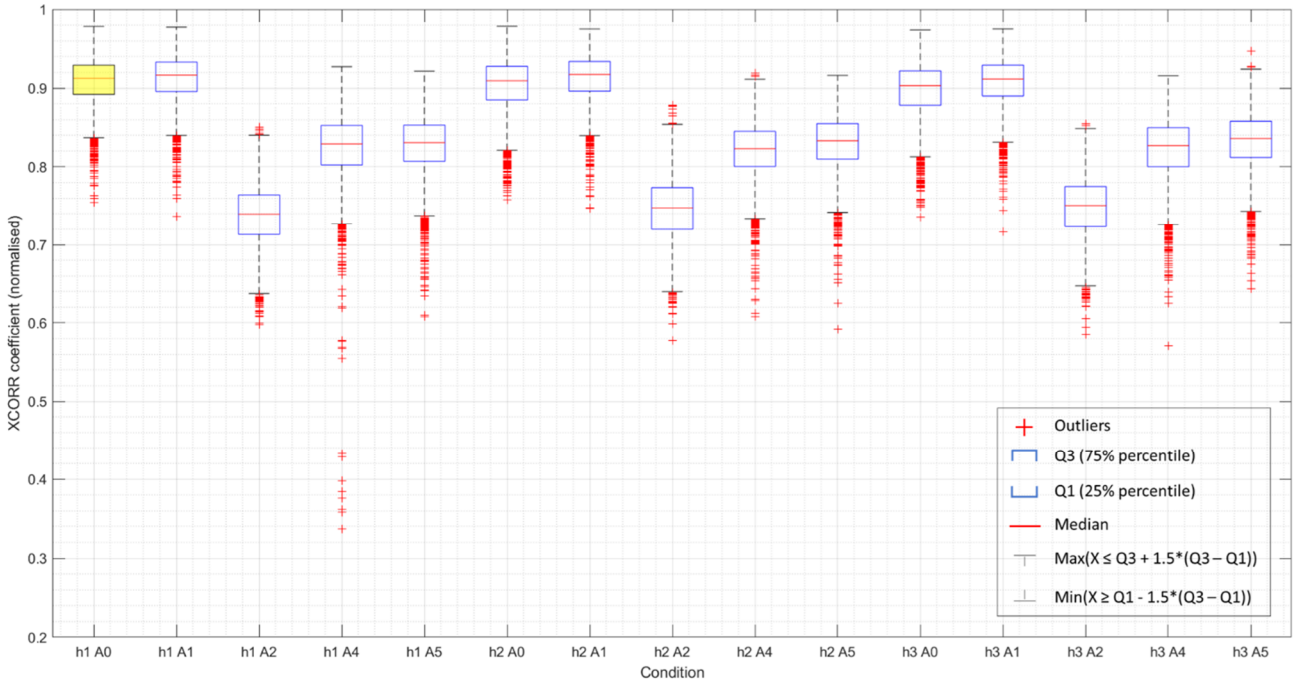

Figure 24. Cross correlation of lower envelope curves of the brake part of the hit after applying a low-pass filter of 200Hz. Hit 1 measured by A0 (h1 A0) is the reference condition, indicated by the yellow box.

In the second step it was found that the sensors whose standard envelope curves showed the highest cross-correlations with curves of the condition they were trying to mimic and the lowest with those of different conditions were A4 for clutch part, A5 for forging part, and A1 for brake part. The values of cross-correlation obtained are shown in Figure 25 (clutch part); Figure 26, Figure 27, and Figure 28 (forging part, one for each of the three hits); and Figure 29 (brake part).

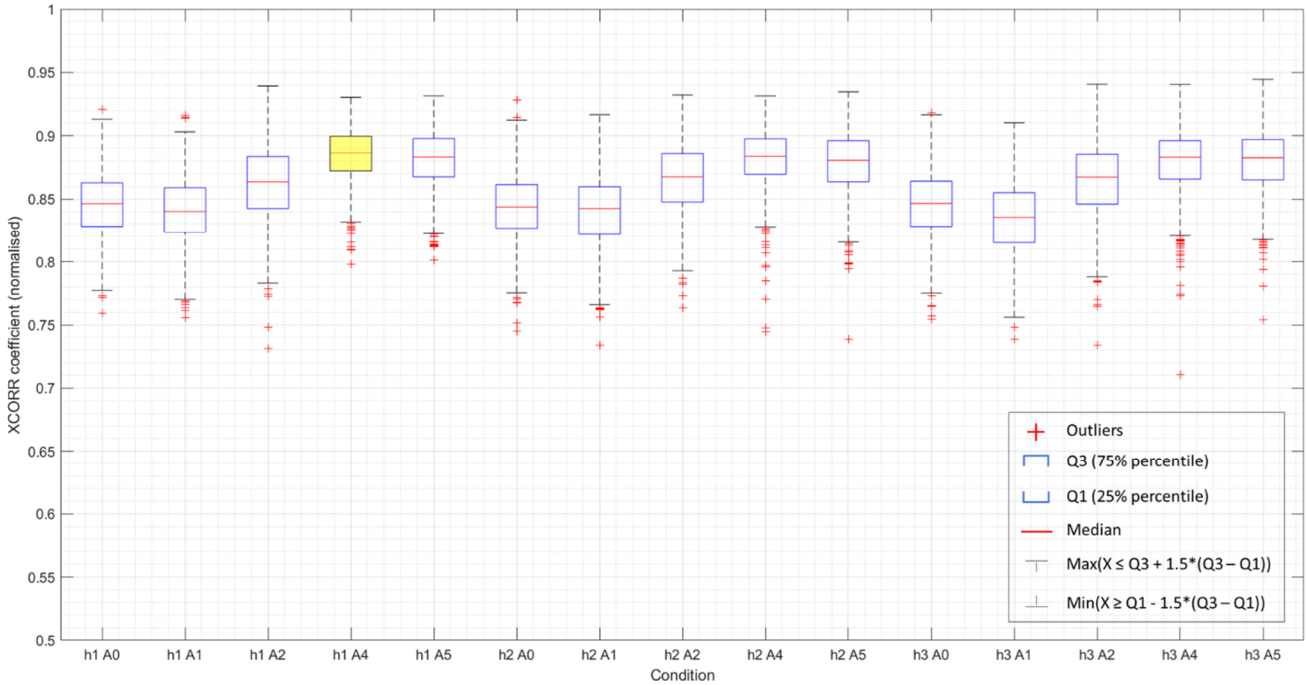

Figure 25. Cross correlations of the lower envelopes of the clutch part of the hit with the standard lower envelope curve of hit 1 measured by A4, after applying a low-pass filter of 200Hz. The condition after which the standard curve is created is indicated by the yellow box.

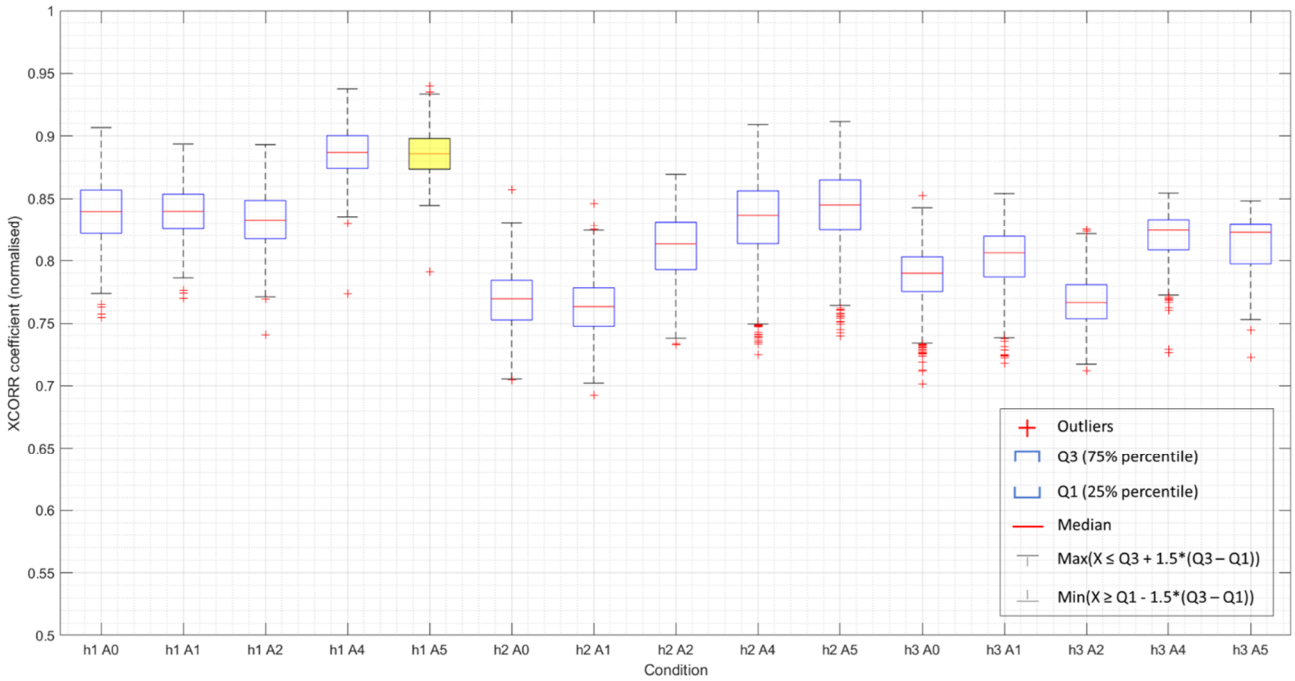

Figure 26. Cross correlations of the lower envelopes of the forging part of the hit with the standard lower envelope curve of hit 1 measured by A5, after applying a low-pass filter of 200Hz. The condition after which the standard curve is created is indicated by the yellow box.

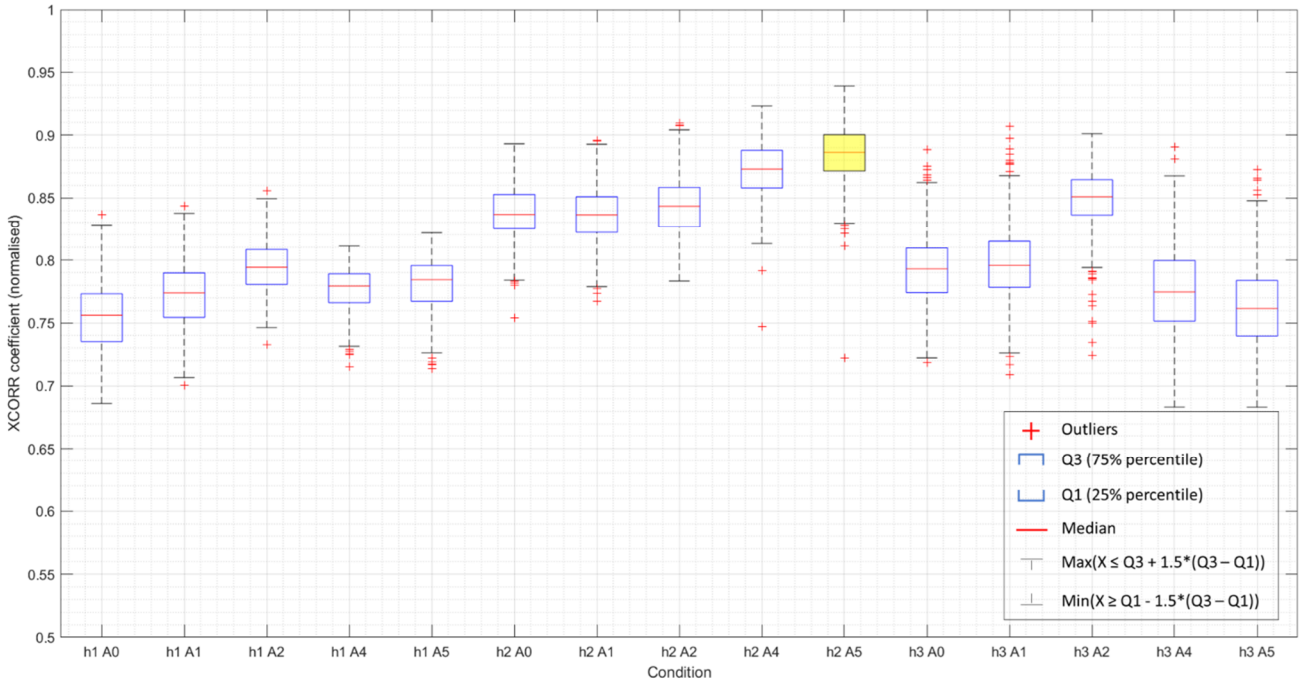

Figure 27.Cross correlations of the lower envelopes of the forging part of the hit with the standard lower envelope curve of hit 2 measured by A5, after applying a low-pass filter of 200Hz. The condition after which the standard curve is created is indicated by the yellow box.

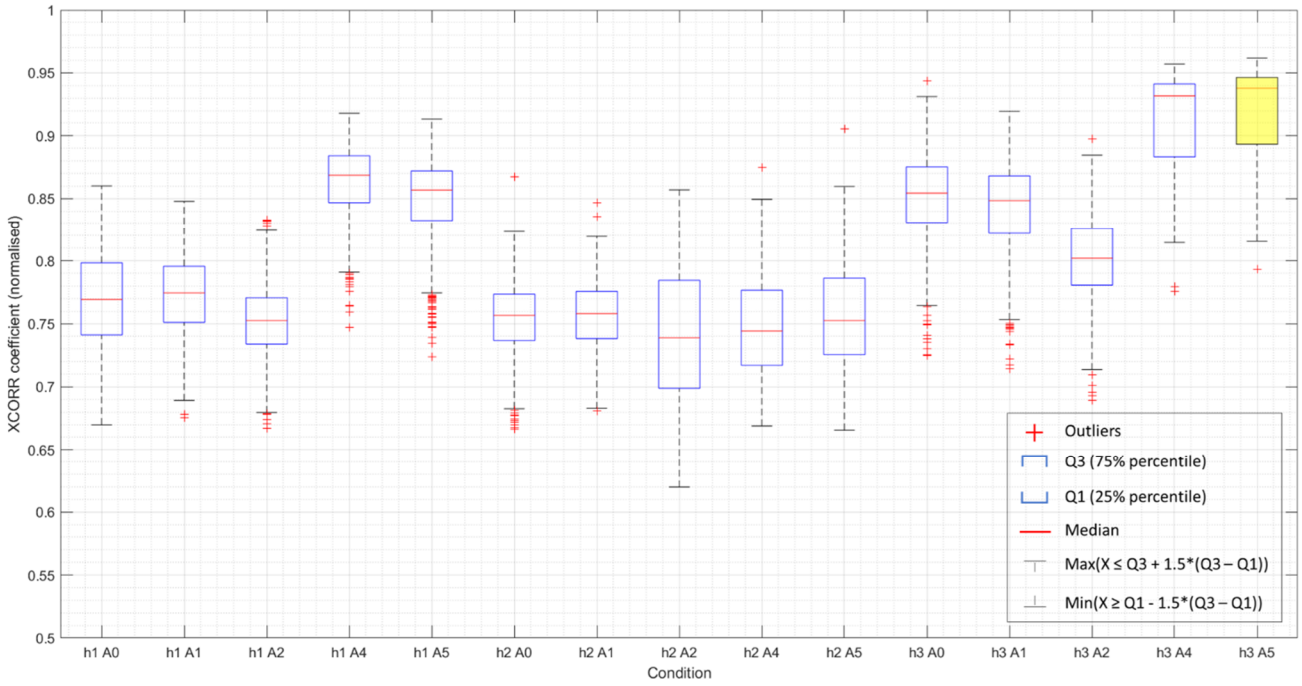

Figure 28. Cross correlations of the lower envelopes of the forging part of the hit with the standard lower envelope curve of hit 3 measured by A5, after applying a low-pass filter of 200Hz. The condition after which the standard curve is created is indicated by the yellow box.

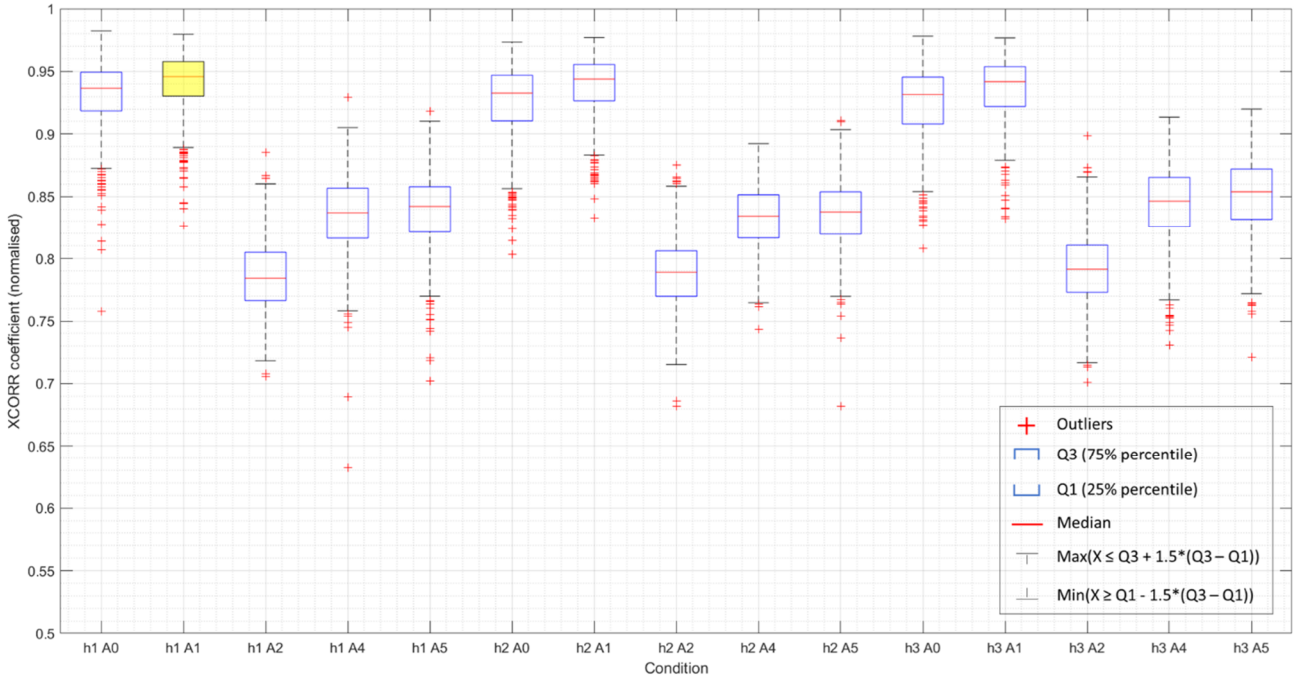

Figure 29. Cross correlations of the lower envelopes of the brake part of the hit with the standard lower envelope curve of hit 1 measured by A1, after applying a low-pass filter of 200Hz. The condition after which the standard curve is created is indicated by the yellow box.

3.3. Features in the frequency domain

The results shown in this section are similar to those of section 3.2 regarding time domain features, although the features in the frequency domain showed narrower intervals. Again, the intervals calculated as $\mu \pm 2\sigma$ contained most of the features for all possible conditions, as can be seen in Table 4. These percentages always remained above 90% when applying the bootstrap sampling method described in section 2.3.

	FC	RMSF	RVF
Minimum	93.76%	93.89%	94.15%
Maximum	99.48%	99.35%	99.61%
Mean	95.67%	95.71%	95.71%
Median	95.58%	95.71%	95.64%
Standard deviation	0.79%	0.80%	0.74%

Table 4. Statistics of the percentage of measurements' frequency-domain features contained between $\mu \pm 2\sigma$

The ratio σ/μ was lower than 20% for all measurements, parts, and conditions, except for the no-filter and low-pass filter conditions for the brake part of the hit measured by sensors A0 and A1. The RVF did not reflect this as much as the FC and the RMSF. This difference can be seen in Figure 30 and Figure 31. It can also be appreciated how the intervals are narrower than those of the features in the time domain: for example, almost all σ/μ ratios in Figure 21 are above 10%, while more than half of those in Figure 31 are below that value.

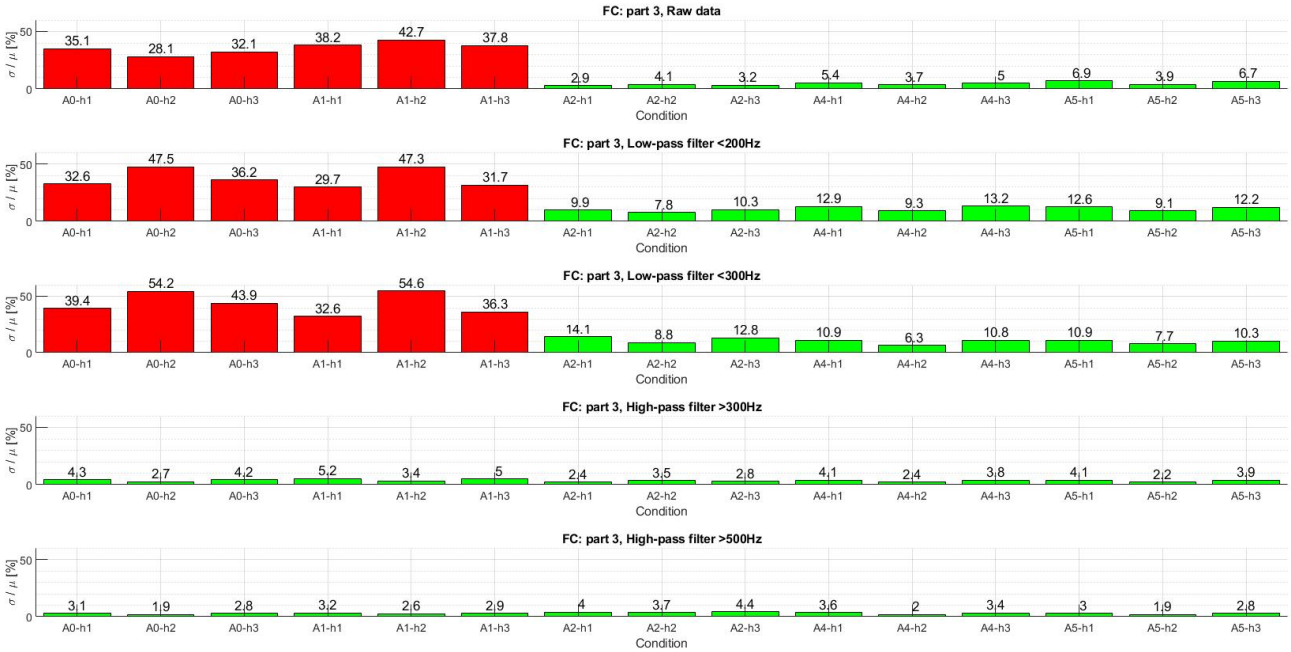

Figure 30. σ/μ ratios for FC in the brake part of the hit

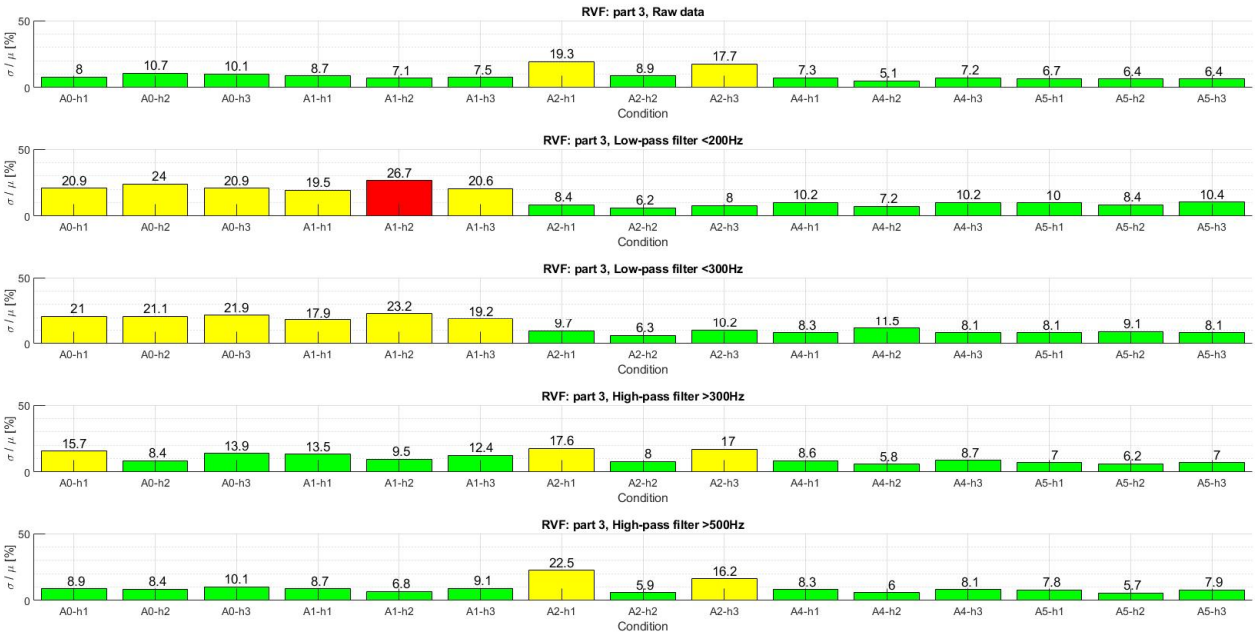

Figure 31. σ/μ ratios for RVF in the brake part of the hit

The different values taken by the features on each measurement can be seen in Figure 32, Figure 33 and Figure 34. Hit number did not show a relevant influence on the frequency domain features, so only those obtained from the first hit are shown. Figure 32 and Figure 33 show that FC and RMSF are almost equivalent. These two figures also show that middle frequencies (between 300 and 600 Hz) are the dominant ones for all parts and sensors, except for the brake part measured by A0 and A1: as it was explained in section 3.1, those sensors detected an important low-frequency component in the brake part of the hit. RVF is similar for all sensors and parts, with the exception being A4 and A5 in the clutch part (higher than the others), and A2 in the brake part (lower) (Figure 34).

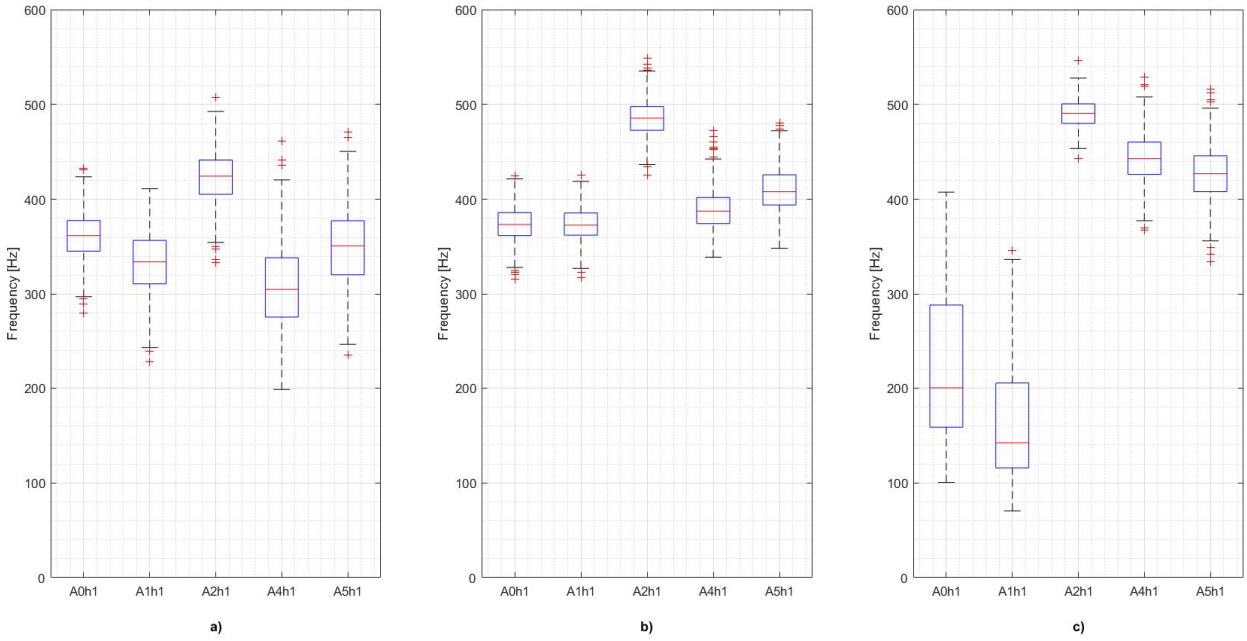

Figure 32. FC values obtained from the first hit for a) clutch part, b) forging part, and c) brake part

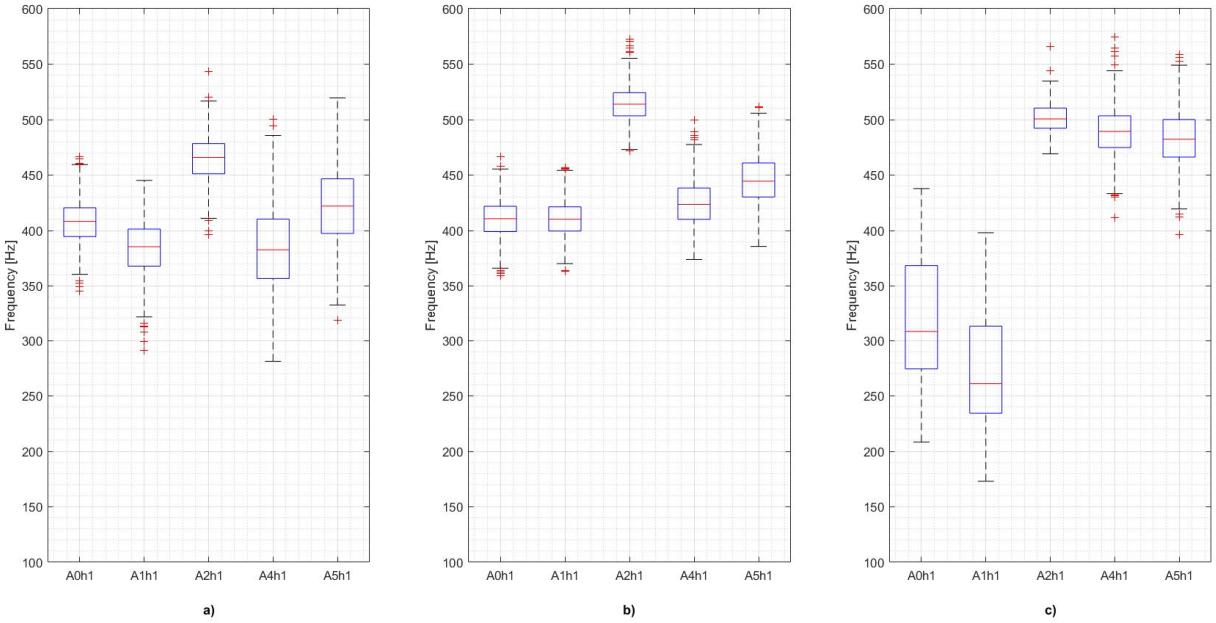

Figure 33. RMSF values obtained from the first hit for a) clutch part, b) forging part, and c) brake part

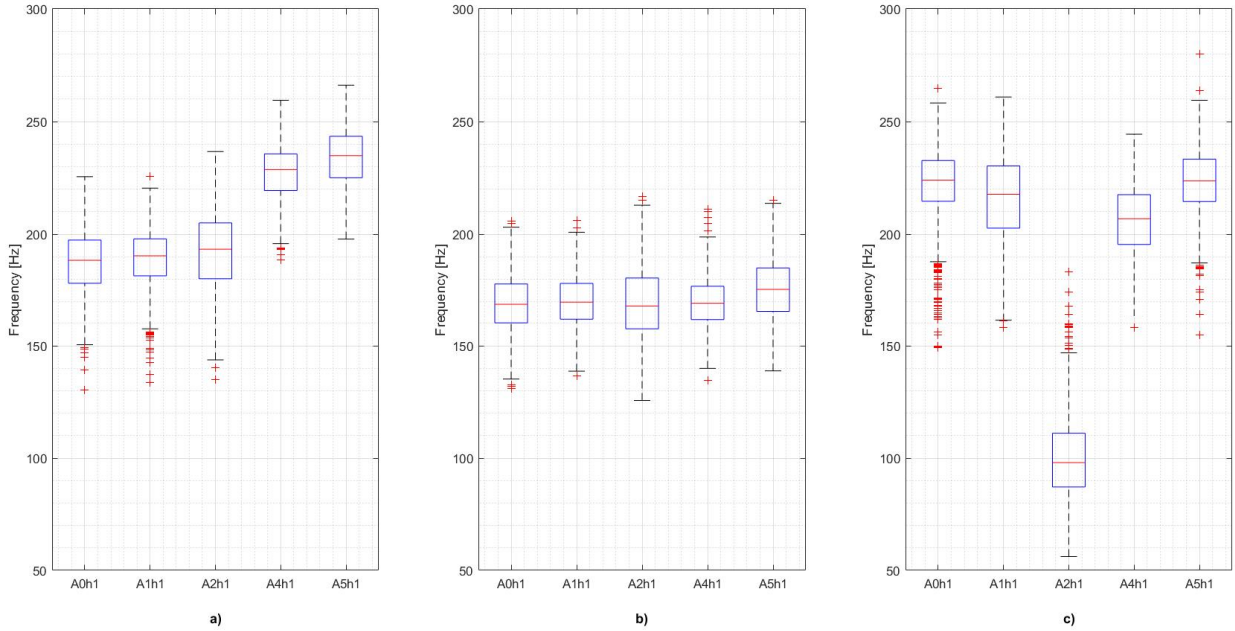

Figure 34. RVF values obtained from the first for a) clutch part, b) forging part, and c) brake part

3.4. Time-frequency domain: STFT

Two examples of STFT plots of a first and a third hit can be seen in Figure 35 and Figure 36. The results presented in section 3.1 can also be appreciated in the STFT: the separation of the hit in 3 parts, the separation of forging part and brake part in two halves, and the dominant low frequencies in the brake part. This is further discussed in section 0.

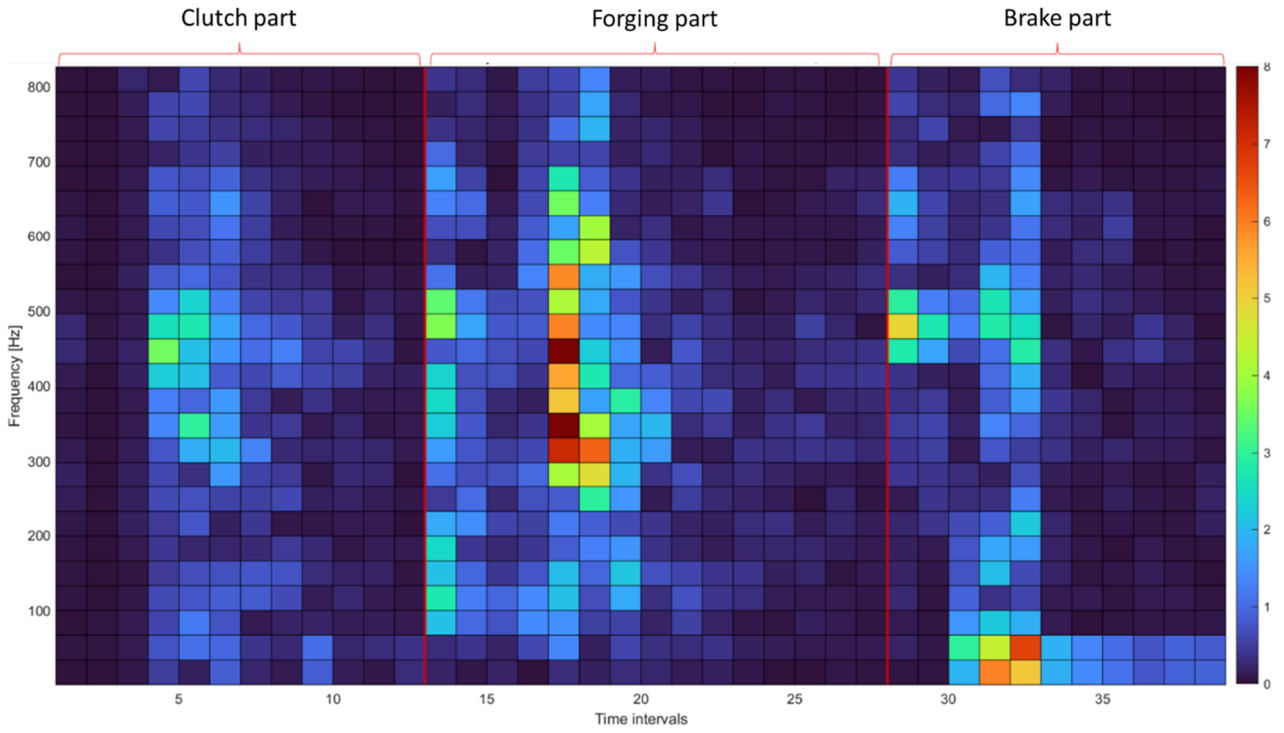

Figure 35. Example of STFT of hit 1 measured by A0

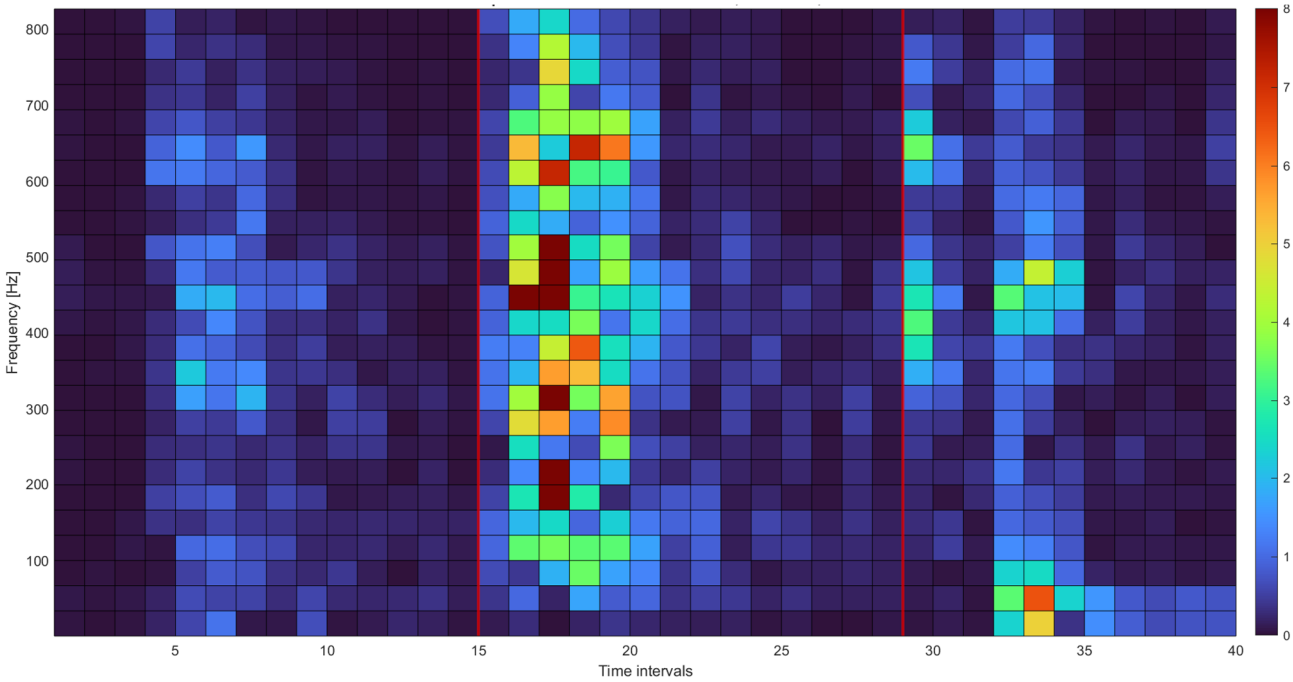

Figure 36. Example of STFT of hit 3 measured by A0

4. Discussion

4.1. Time domain data

The hits corresponding to each of the 3 stages of the press could be seen clearly from the initial measurements (Figure 9). The only exception was those taken from sensor A3, which reached saturation consistently through all its measurements, probably because of it being located too close to the brake of the machine.

As was shown in Figure 10 and Figure 11 the number of 3-hits groups per measurement was not constant. This caused time intervals between groups to not be constant either, which made it necessary to develop the algorithm to locate them.

Each of the parts of the hit shown in Figure 12 had a different origin. The first part (clutch part) was caused by the beginning of the torque transmission from the flywheel through the clutch and the start of the movement of the shaft. The second one (forging part) was caused by the hit itself and the forging of the workpiece. The third (brake part) was caused by the arrival of the ram to the top dead centre position and the brake of the machine. A fourth part was found only in the second hit, caused by a switch in the press configuration to prepare for the last hit.

The clutch part had a small non-centred in 0 component (Figure 17) formed mainly by low frequencies (<300Hz), detected only by sensors A0 and A1. This occurred because the clutch acted in the horizontal direction, and sensors A0 and A1 were the only ones oriented in said direction.

The division of the forging part in two halves was expected, as the forming force required to forge a workpiece is not constant throughout the deformation, but it has a non-linear relation with the ram path and the deformation itself. As shown in Figure 37 [10], a high peak is found in the forming force at the end of the forging, caused by the friction between the working material and the die walls [17]. This explains the presence of the two halves of the part: the first one corresponds to the initial contact between the ram and the workpiece, the second one is caused by the friction with the die walls, and the "space" between halves by the deformation of the billet without friction with the walls. The change in the shape of this part as the hits advance from the first to the third would be caused by the reduction of the "deformation without wall friction" phase in the last hits, as the workpiece is closer to its final geometry. This part of the hit is always stronger in the third hit, which is also explained by this: as the workpiece gets closer to its final shape more friction with the die walls is required in the forging process.

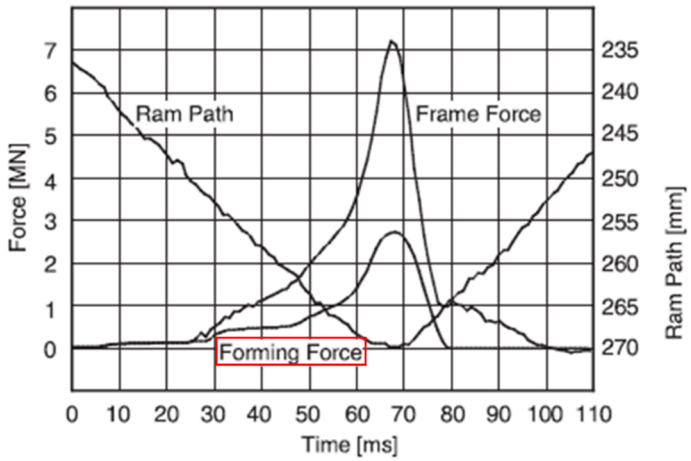

Figure 37. Evolution of the forming force with time and ram path [10]

The origin of the first half of the brake part of the hit was the arrival of the ram to the TDC position, while the second half was caused by the action of the brake (Figure 14). In a similar way to what happened with the clutch part, A0 and A1 were the only ones able to detect the second half of the part because they were oriented in the horizontal direction, in which the brake acted.

4.2. Features in the time domain

Given that more than 90% of all measurements' time domain features were contained within their $\mu \pm 2\sigma$ intervals (Table 3), features being consistently outside of said intervals can be considered a sign of non-nominal working conditions. An example of this would be to set an alarm when 10 or more consecutive measurements show features outside the intervals, or when 15% or more measurements in a one-hour window do it. However, those intervals alone would not be enough to monitor if the machine is working under regular conditions or not. The reason for this can be seen in Figure 19, in which the RMS of the low frequency component measured by A1 in the brake part of the hit is shown. Even though the RMS is mostly between bounds, the working conditions of the brake are clearly changing through the day, and all measurements are inside of the interval simply because the standard deviation of the data is too big (and so is the interval itself). While this variation in working conditions cannot be considered problematic, as no issues were found by the company regarding the brake of the machine, it suggests that the intervals of RMS of this part would be too wide to detect a significant deviation from nominal conditions. This is why narrow intervals ($\sigma/\mu<25\%$) were preferred.

σ/μ ratios where especially high for sensors A0 and A1 without high-pass filters (>300Hz or higher) when monitoring RMS in the brake part of the hit, reaching 44% (Figure 20). However, this occurred because the change in operating conditions in that part was detected only by those sensors in the low frequencies. As stated before, operating conditions of the brake part of the hit changed through the measurements, so sensors and filters that did not show it (A2, A4 and A5 regarding sensors, and high-pass filters) should not be considered a valid choice for monitoring it.

While the increase in ratios can be clearly seen for RMS of brake part in A0 and A1 when high-pass filters are not applied (Figure 20), the same does not occur with crest factor (Figure 21), which indicates that this feature could be interesting for monitoring the brake part of the hit.

All intervals had positive lower bounds for kurtosis, which means that negative kurtosis could be a sign of non-nominal situations. Regarding skewness, it was not clearly positive nor negative for any condition, so the monitoring of this feature was not considered a priority.

To summarize, the features in the time domain of the clutch and forging parts of the hit could be monitored with both RMS and crest factor intervals applied to non-filtered signals measured by sensors A0, A1 or A2. The brake part of the hit could be monitored with crest factor intervals applied to low-pass filtered signals acquired by A0 or A1. Positive kurtosis should be expected in at least 90% of the measurements, so measurements with negative kurtosis should be treated as an out-of-intervals one. An example of the intervals for RMS and crest can be seen in Table 5, showing the expected bounds for sensor A1.

Part	Hit	Frequency filter	RMS [m/s^2]			Crest factor		
			Min.	Max.	σ/μ [%]	Min.	Max.	σ/μ [%]
Clutch	1st	None	2.51	4.94	16.2	3.79	7.01	14.9
Forging	1st	None	6.65	9.22	8.1	4.32	8.53	16.4
	2nd	None	8.29	11.44	8.0	4.11	7.33	14.1
	3rd	None	10.89	17.93	12.2	4.37	9.43	18.3
Brake	1st	<200 Hz	-	-	-	3.41	6.28	14.8

Table 5. RMS and crest factor intervals for sensor A1

4.2.1. Envelope analysis

The first step of envelope analysis showed that:

- Cross-correlation between curves of clutch part does not depend on hit number, only on sensor. The same occurs between curves of brake part.
- Cross-correlation between curves of forging part depends on both hit number and sensor.
- Higher cross-correlation is found when comparing the lower envelope instead of the upper one.
- Higher cross-correlation is found for all parts when applying low pass filters.
- Clutch and forging parts are better monitored by sensors A4 and A5.
- Brake part is better monitored by sensor A0 and A1.

These conclusions agree with section 2.3.1: as the clutch and brake parts of the hit are caused by the clutch, the brake, and the beginning and end of the movement of the ram, they are not related with the stage of the press being used. Figure 22 and Figure 24 show how the cross-correlations between curves of the same hit reach almost identical values as those between curves of different ones, as long as they are measured by the same sensors. The forging part is caused by the hit itself, so it will depend on it, as can be seen in Figure 23.

The importance of low-frequency components in the shape of the curves was also shown in section 2.3.1., and it is the reason for low-pass filtered signals being easier to understand through the shape of their envelopes. It can also be appreciated how sensors A0 and A1 on one hand, and A4 and A5 on the other, show very similar results (from Figure 22 to Figure 29), so they could be considered redundant.

When applying the second step it was found that the sensors more adequate to monitor each part of the hit were A4 for clutch part, A5 for forging part, and A1 for brake part. This conclusion was drawn because their standard envelope curves showed the highest cross-correlation with the curves of the condition they were modelled after, while obtaining lower cross-correlation values with curves of other conditions (section 3.2.1). Monitoring any of the 3 hits would be enough for clutch and brake parts, as they do not depend on the hit, but forging part would require monitoring all three of them. Results for these sensors are shown from Figure 25 to Figure 29, were it can be seen that, despite the big variability found in the data, the cross-correlations between the standard curves and the condition they are trying to mimic is clearly higher than the one obtained against the other conditions. This method works particularly well for the brake part of the hit (Figure 29).

A way to implement this idea could be to use the lowest cross-correlation reached between the standard curves and their condition as a threshold (Table 6). If cross-correlation between new measurements and their standard envelope curves were repeatedly lower than said thresholds, it would be a sign of the behaviour of the machine not being the nominal one. Given the big variability of the data, this monitoring method should be applied by evaluating a large set of measurements (for example, those taken during a whole working day), and the detection of non-nominal conditions should only be considered if a relevant number of them (for example, 10%) showed cross-correlations lower than the threshold.

Part	Hit	Sensor	Threshold
Clutch	Any	A4	80%
Forging	1	A5	84%
	2	A5	80%
	3	A5	80%
Brake	Any	A1	82%

Table 6. Minimum thresholds for cross-correlation with standard envelope curves

4.3. Frequency domain features

The intervals of the features in the frequency domain contained most of the measurements (Table 4), and their intervals were narrower than those of the features in the time-domain, which made them appropriate for complementing the features in the time domain and the envelope at monitoring the machine.

As it was shown in section 3.3, FC and RMSF showed increased σ/μ ratios for low-pass and non-filtered measurements of brake part recorded by A0 and A1 (Figure 30), while RVF did not reflect this as much (Figure 31). This indicates that the change in operating conditions in the brake part also affects the frequency domain, and that, while the frequencies of the main bands are strongly affected by this change, the distribution of energy in the power spectrum with respect to said main bands does not change as much. The situation is similar to the one involving RMS and crest factor explained in section 4.2: the detected change in operating conditions in the brake part is not problematic, but the interval of FC is so wide that it would probably not be able to detect a significant deviation from nominal conditions, which is why RVF would be more adequate than FC to monitor that part of the hit.

Higher RVF indicates higher dispersion of energy around the frequency centre FC, which means a lower RVF is preferred for monitoring. RVF in clutch part was higher for A4 and A5, and lower in brake part for A2 (Figure 34). However, A2 is unable to measure the low-frequency components of the brake part, so it would not be a valid choice; and A4 and A5 showed above-average performance when monitoring envelope shape (section 3.2.1), so they should not be discarded either.

The results regarding FC and RMSF were almost identical, so it would be enough to just focus on FC and RVF. As usual, it would be needed to use either A0 or A1 for monitoring the brake part of the hit, but the other two parts could be monitored by any of the five sensors. Hit number (first, second, or third) did not show a relevant influence in the frequency domain features, so monitoring any of the three would be adequate. A good strategy would be to monitor both time and frequency domain of each part with the same sensors, as this would increase the possibilities of early detecting any deviation from nominal conditions. It would be better to extract the features in the frequency domain without applying frequency filters, as this would allow to monitor the higher frequencies that won't be seen if applying low-pass filters on time-domain features and envelope analysis. An example of the expected intervals for FC and RVF can be seen in Table 7, showing the expected bounds for sensor A1.

Part	Hit	FC [Hz]			RVF [Hz]		
		Min.	Max.	σ/μ [%]	Min.	Max.	σ/μ [%]
Clutch	1st	268	398	9.7	163	215	7.0
Forging	1st	337	409	4.8	146	194	7.0
	2nd	332	408	5.1	149	196	6.9
	3rd	349	438	5.6	141	194	7.9
Brake	1st	-	-	-	179	254	8.7

Table 7. FC and RVF intervals for sensor A1

4.4. STFT

The separation of the forging and brake part of the hit in two halves pointed out in section 3.1 can be seen in Figure 35, with the first half of the forging part beginning in the 13th time interval and the second half beginning in the 17th, and the first half of the brake part beginning in the 28th and the second half beginning in the 30th. The low-frequency component of the brake part can also be seen, being it the main component of the second half of the brake part.

The stronger frequencies of clutch and forging parts are in the range of 250 Hz to 550 Hz, while the brake part has a first half made of those same frequencies, and a second half whose dominant frequencies are below 100 Hz. This is coherent with the results found in section 4.2, and is particularly clear when looking at the frequency centre of the different parts of the hit (Figure 32).

The big variability of the FC of the brake part measured by A0 and A1 can be explained by the wide difference in the frequency components of the two halves of said part, and by the big variability of the data. The relationship between the intensity of the two halves is not constant across the data, which is the reason for the FC of those conditions changing in a range that wide (between 100 Hz and 400 Hz for A0).

When comparing Figure 35 with Figure 36, it can be appreciated how the separation in two halves of the forging part disappears in the third hit, while it can be seen clearly in the first one.

5. Conclusions

The nominal working conditions of an eccentric mechanical press with three stages used in a hot forging process were characterized through the analysis of its vibrations, measured with six piezoelectric accelerometers distributed through the machine. The vibrations caused by each hit in each stage of the press were divided in 3 different parts, and the origin of each part was discussed in detail. It was found that having at least 1 accelerometer oriented in the direction in which the clutch and the brake were acting (in this work, A0 and A1) was essential for monitoring the machine, as sensors oriented perpendicularly to those components were unable to detect changes in their operating conditions.

The features that allowed for the characterization were RMS, crest factor, and kurtosis in the time-domain; and frequency centre and root variance frequency in the frequency domain. A set of intervals with lower and upper bounds were created for each feature. It was found that at least 90% of measurements' features were contained inside those intervals, and an example of them was proposed to monitor the time and frequency domain features needing only one accelerometer.

The shape of the envelope of the recorded signals was analysed using the cross-correlation function, and standard envelope curves were created for each sensor, stage, part of the hit, and frequency filtering condition. The standard curves proved useful for monitoring the shape of the envelope, and minimum thresholds for the cross-correlation between those standard curves and future new measurements were set. The procedure for monitoring the shape of the envelope worked best when applying a low-pass filter of 200 Hz to the acceleration signals. A monitoring strategy was proposed, which needed two additional accelerometers.

Regarding future investigations, it would be interesting to use STFT or other time-frequency domain transforms to perform part classification. That is, image analysis could be applied to STFT spectrograms in order to classify the pieces produced (and thus the measurements) in clusters with common time-frequency domain behaviour, allowing to reduce the variability of the data by studying each cluster individually. Measuring other variables, such as forces or temperatures, and analysing their relationship with the vibrations, could be useful too.

6. References

[1] S. Kalpakjian *et al.*, *MANUFACTURING ENGINEERING AND TECHNOLOGY*, Sixth Edition. Pearson, 2010.

[2] "Eccentric Press (Glass Mosaic) | 3D CAD Model Library | GrabCAD." https://grabcad.com/library/eccentric-press-glass-mosaic-1 (accessed Jan. 24, 2022).

[3] E. Rusinski, P. Harnatkiewicz, G. Przybyłek, and P. Moczko, "Analysis of the fatigue fractures in the eccentric press shaft," *Solid State Phenom.*, vol. 165, pp. 321–329, 2010.

[4] P. Hamrle and J. Hlaváč, "Load analysis of crankshaft of two-point crank press," in *Annals of DAAAM and Proceedings of the International DAAAM Symposium*, 2018, vol. 29, no. 1, pp. 0601–0608, doi: 10.2507/29th.daaam.proceedings.087.

[5] R. K. Mobley, *An introduction to predictive maintenance*. Butterworth-Heinemann, 2002.

[6] P. V. Torres-Carrion, C. S. Gonzalez-Gonzalez, S. Aciar, and G. Rodriguez-Morales, "Methodology for systematic literature review applied to engineering and education," *IEEE Glob. Eng. Educ. Conf. EDUCON*, vol. 2018-April, pp. 1364–1373, May 2018, doi: 10.1109/EDUCON.2018.8363388.

[7] C. Durand, L. Freund, C. Baudouin, R. Bigot, and J.-D. Guérin, "Comparison of different sensor technologies to monitor a forging process," *ESAFORM 2021*, Apr. 2021, doi: 10.25518/esaform21.1475.

[8] S. A. Spiewak, R. Duggirala, and K. Barnett, "Predictive monitoring and control of the cold extrusion process," *CIRP Ann. - Manuf. Technol.*, vol. 49, no. 1, pp. 383–386, 2000, doi: 10.1016/S0007-8506(07)62970-9.

[9] K. Barnett, R. Duggirala, D. Hitz, and S. Spiewak, "Monitoring and Control of Equipment and Process in Cold Extrusion," *J. Mater. Manuf.*, vol. 107, pp. 991–1001, 1998.

[10] E. Doege, F. Meiners, T. Mende, W. Strache, and J. W. Yun, "Sensors for Process Monitoring: Metal Forming," *Sensors Appl.*, vol. 1, pp. 172–202, Feb. 2008, doi: 10.1002/9783527619252.CH4B.

[11] M. Hawryluk, J. Ziemba, and P. Sadowski, "A Review of Current and New Measurement Techniques Used in Hot Die Forging Processes," *Measurement and Control (United Kingdom)*, vol. 50, no. 3. SAGE Publications Ltd, pp. 74–86, Apr. 01, 2017, doi: 10.1177/0020294017707161.

[12] T. A. Dean and T. M. Silva, "Die temperatures during production drop forging," *J. Manuf. Sci. Eng. Trans. ASME*, vol. 101, no. 4, pp. 385–390, 1979, doi: 10.1115/1.3439524.

[13] M. Terčelj, R. Turk, and M. Knap, "Assessment of temperature on the die surface in laboratory hot metal forming," *Appl. Therm. Eng.*, vol. 23, no. 2, pp. 113–125, Feb. 2003, doi: 10.1016/S1359-4311(02)00170-9.

[14] P. Dadras and W. R. Wells, "Heat transfer aspects of nonisothermal axisymmetric upset forging," *J. Manuf. Sci. Eng. Trans. ASME*, vol. 106, no. 3, pp. 187–195, 1984, doi: 10.1115/1.3185932.

[15] M. A. Kellow, A. N. Bramley, and F. K. Bannister, "The measurement of temperatures in forging dies," *Int. J. Mach. Tool Des. Res.*, vol. 9, no. 3, pp. 239–260, 1969, doi: 10.1016/0020-7357(69)90002-X.

[16] D. M. Ştefănescu, "Strain gauges and Wheatstone bridges - Basic instrumentation and new applications for electrical measurement of non-electrical quantities," 2011, doi: 10.1109/SSD.2011.5767428.

[17] A. O. A. Ibhadode and T. A. Dean, "Simulation and experimental verification of completely closed cavity die forging on a mechanical press," *Proc. Inst. Mech. Eng. Part B J. Eng. Manuf.*, vol. 203, no. 1, pp. 17–32, 1989, doi: 10.1243/PIME_PROC_1989_203_042_02.

[18] S. A. Balogun, "Determination of deformation forces in cavity press forging," *Met. Technol.*, vol. 1, no. 1, pp. 375–380, Aug. 1974, doi: 10.1179/030716974803287843.

[19] L. X. Kong and S. Nahavandi, "On-line tool condition monitoring and control system in forging processes," 2002, doi: 10.1016/S0924-0136(02)00367-9.

[20] E. Doege and R. Bohnsack, "Closed die technologies for hot forging," *J. Mater. Process. Technol.*, vol. 98, no. 2, pp. 165–170, Jan. 2000, doi: 10.1016/S0924-0136(99)00194-6.

[21] M. H. Sadeghi and T. A. Dean, "Analysis of ejection in precision forging," *Int. J. Mach. Tools Manuf.*, vol. 30, no. 4, pp. 509–519, Jan. 1990, doi: 10.1016/0890-6955(90)90003-2.

[22] E. Doege, J. Baumgarten, and T. Neumaier, "The Concept of Active Deflection Compensation and its Application in Precision Forging," in *Initiatives of Precision Engineering at the Beginning of a Millennium*, Springer, Boston, MA, 2002, pp. 27–31.

[23] C. K. Mukhopadhyay *et al.*, "Optimization of positioning of an acoustic emission sensor for monitoring hot forging," *Mater. Manuf. Process.*, vol. 21, no. 5, pp. 543–549, Jun. 2006, doi: 10.1080/10426910500471698.

[24] I. El-Galy and B.-A. Behrens, "Online Monitoring of Hot Die Forging Processes Using Acoustic Emission (Part-I)," *J. Acoust. Emiss.*, vol. 26, pp. 208–219, 2008, Accessed: Feb. 21, 2022. [Online]. Available: https://www.researchgate.net/publication/263315079_Online_Monitoring_of_Hot_Die_Forging_Processes_Using_Acoustic_Emission_Part-I.

[25] M. Hawryluk, M. Kaszuba, Z. Gronostajski, and P. Sadowski, "Systems of supervision and analysis of industrial forging processes," *Eksploat. i Niezawodn.*, vol. 18, no. 3, pp. 315–324, 2016, doi: 10.17531/ein.2016.3.1.

[26] R. B. Randall, *Vibration-Based Condition Monitoring: Industrial, Aerospace and Automotive Applications*. wiley, 2010.

[27] S. Erkaya and I. Uzmay, "Experimental investigation of joint clearance effects on the dynamics of a slider-crank mechanism," *Multibody Syst. Dyn. 2010 241*, vol. 24, no. 1, pp. 81–102, Feb. 2010, doi: 10.1007/S11044-010-9192-0.

[28] E. Zheng and X. Zhou, "Modeling and simulation of flexible slider-crank mechanism with clearance for a closed high speed press system," *Mech. Mach. Theory*, vol. 74, pp. 10–30, Apr. 2014, doi: 10.1016/J.MECHMACHTHEORY.2013.11.015.

[29] E. Salahshoor, S. Ebrahimi, and Y. Zhang, "Frequency analysis of a typical planar flexible multibody system with joint clearances," *Mech. Mach. Theory*, vol. 126, pp. 429–456, Aug. 2018, doi: 10.1016/J.MECHMACHTHEORY.2018.04.027.

[30] T. Xu, Q. Xia, X. Long, and G. Buffa, "Vibration Control of a High-Speed Precision Servo Numerically Controlled Punching Press: Multidomain Simulation and Experiments," *Shock Vib.*, vol. 2017, 2017, doi: 10.1155/2017/4593546.

[31] A. Glaeser *et al.*, "Remote machine mode detection in cold forging using vibration signal," vol. 48, pp. 908–914, 2020, doi: 10.1016/J.PROMFG.2020.05.129.

[32] A. Glaeser *et al.*, "Applications of deep learning for fault detection in industrial cold forging," *https://doi.org/10.1080/00207543.2021.1891318*, vol. 59, no. 16, pp. 4826–4835, 2021, doi: 10.1080/00207543.2021.1891318.

[33] W. Caesarendra and T. Tjahjowidodo, "A Review of Feature Extraction Methods in Vibration-Based Condition Monitoring and Its Application for Degradation Trend Estimation of Low-Speed Slew Bearing," *Mach. 2017, Vol. 5, Page 21*, vol. 5, no. 4, p. 21, Sep. 2017, doi: 10.3390/MACHINES5040021.

[34] "ISO - ISO 10816-6:1995 - Mechanical vibration — Evaluation of machine vibration by measurements on non-rotating parts — Part 6: Reciprocating machines with power ratings above 100 kW." Accessed: Feb. 28, 2022. [Online]. Available: https://bsol.bsigroup.com/.

[35] R. B. Randall and J. Antoni, "Rolling element bearing diagnostics-A tutorial," *Mech. Syst. Signal Process.*, vol. 25, no. 2, pp. 485–520, 2011, doi: 10.1016/J.YMSSP.2010.07.017.

[36] W. Shen and C. Ai, "On-line monitoring methodology for die forging quality based on the piezoelectric effect," *Proc. World Congr. Intell. Control Autom.*, pp. 4173–4177, 2010, doi: 10.1109/WCICA.2010.5554960.

[37] O.-S. Yang and A. Widodo, *Introduction of intelligent machine fault diagnosis and prognosis*. 2009.

[38] B. Ryden, "Predictive Maintenance with Vibration Sensors White Paper | TE Connectivity," 2021. https://www.te.com/usa-en/industries/sensor-solutions/insights/condition-monitoring-white-paper.html (accessed Feb. 13, 2022).

[39] S. J. Lacey, "The Role of Vibration Monitoring in Predictive Maintenance," *Maint. Asset Manag.*, vol. 25, no. 2, pp. 38–44, 2010.

[40] S. R. Hayashi, C. E. Thomas, D. G. Wildes, and G. Tlusty, "Tool Break Detection by Monitoring Ultrasonic Vibrations," *CIRP Ann.*, vol. 37, no. 1, pp. 61–64, Jan. 1988, doi: 10.1016/S0007-8506(07)61586-8.

[41] "Zar, Biostatistical Analysis, 5th Edition | Pearson." https://www.pearson.com/us/higher-education/program/Zar-Biostatistical-Analysis-5th-Edition/PGM263783.html (accessed Mar. 19, 2022).

7. Abstract in lingua italiana

Questo lavoro applica l'analisi delle vibrazioni per caratterizzare le condizioni di lavoro nominali di una pressa eccentrica a tre stadi utilizzata in un processo di forgiatura a caldo. La caratterizzazione è ottenuta con successo attraverso l'analisi delle features del dominio temporale, del dominio della frequenza, e dell'analisi dell'inviluppo. Viene studiata l'origine di ciascuno dei segnali di vibrazione registrati e vengono discussi i vantaggi di diversi filtri di frequenza e posizioni dei sensori. Infine, viene proposta una strategia di monitoraggio del processo di forgiatura.

Parole chiave: forgiatura, manutenzione predittiva, vibrazione, manutenzione secondo condizione